JOURNAL OF GEOPHYSICAL RESEARCH, VOL. 114, A12301, doi:10.1029/2009JA014259, 2009

Nightside ionospheric electrodynamics associated with substorms: PFISR and THEMIS ASI observations

S. Zou,[1] L. R. Lyons,[1] M. J. Nicolls,[2] C. J. Heinselman,[2] and S. B. Mende[3]

Received 17 March 2009; revised 11 August 2009; accepted 26 August 2009; published 2 December 2009.

[1] Observations from the newly available Poker Flat Incoherent Scatter Radar have been used to study the ionospheric electrodynamics during the substorm expansion phase. Substorm events selected have been divided into three categories based on onset location relative to the radar, and repeatable features have been identified. West of onset, westward flows increased in response to the passage of the westward traveling surge (WTS) poleward of them. The enhanced flows occurred within the Sub-Auroral Polarization Streams region of downward Region 2 currents, which extend equatorward from near the equatorward boundary of electron precipitation. Strong *E* region ionization increase associated with the WTS occurred poleward of the enhanced westward flows, suggesting that poleward Pedersen currents fed by the downward Region 2 field-aligned current (FAC) further equatorward contribute at least partially to closure of the upward FAC of the WTS. An enhanced eastward flow channel developed east of onset. *E* region ionization decreased poleward of this flow peak, implying formation of downward FAC, and further increased equatorward of the flow peak, suggesting strengthening of preexisting Region 2 upward FAC. These observations indicate that the downward FAC formed at onset at least partially closes via the upward Region 2 currents. The enhanced eastward flows decreased after passage of the auroral bulge, and the reduced *E* region ionization increased again. When onset occurred within the radar fov, the thin breakup arc of onset occurred at the center of the Harang reversal, while if the optical onset was poleward of the radar fov, the Harang reversal was observed after the onset. A 2-D picture of the evolution of ionospheric electrodynamics was generated by synthesizing observations from the three categories, which provides a schematic description of the relationship between Region 2 and substorm expansion electrodynamics.

Citation: Zou, S., L. R. Lyons, M. J. Nicolls, C. J. Heinselman, and S. B. Mende (2009), Nightside ionospheric electrodynamics associated with substorms: PFISR and THEMIS ASI observations, *J. Geophys. Res.*, *114*, A12301, doi:10.1029/2009JA014259.

1. Introduction

[2] Substorms are a major geomagnetic disturbance, during which energy stored in the magnetotail during the growth phase is released in an abrupt way after the expansion onset. Dramatic changes occur both in the magnetosphere and in the high latitude ionosphere during substorms. Much research of the ionospheric electrodynamics related to substorm has been performed using various instruments, such as ground-based incoherent/coherent scatter radars [e.g., *Kamide and Vickrey*, 1983; *Robinson et al.*, 1985; *Bristow et al.*, 2001, 2003; *Bristow and Jensen*, 2007; *Liang et al.*, 2006; *Zou et al.*, 2009] and magnetometers [e.g., *McPherron*, 1970; *Rostoker*, 1972; *Tighe and Rostoker*, 1981; *Sergeev et al.*, 1996], as well as in situ observations from low-altitude polar-orbiting satellites [e.g., *Fujii et al.*, 1994; *Hoffman et al.*, 1994; *Gjerloev et al.*, 2003].

[3] In the current paper, we focus on observations of ionospheric electrodynamics during the substorm expansion phase obtained by the newly available Poker Flat Advanced Modular Incoherent Scatter Radar (PFISR). Incoherent Scatter Radar (ISR) is a powerful ground-based tool for studying ionospheric physics owing to its ability to simultaneously measure multiple parameters, such as ion drift velocity (i.e. $\vec{E} \times \vec{B}$ drift), electron density, and electron/ion temperatures, along the line-of-sight (los) direction. In particular, the ion drift velocity and electron density as a function of latitude/altitude are of great interest for studying magnetosphere-ionosphere coupling. The PFISR radar, one of the three faces of the Advanced Modular Incoherent Scatter Radar (AMISR) system, finished assembly and began operating in 2007. There are many advantages of this new instrument. First, it is located at the Poker Flat Research Range near Fairbanks, Alaska with geomagnetic latitude (mlat) ~65.4°, excellent for measuring the electro-

[1]Department of Atmospheric and Oceanic Sciences, University of California, Los Angeles, California, USA.
[2]Center for Geospace Studies, SRI International, Menlo Park, California, USA.
[3]Space Sciences Laboratory, University of California, Berkeley, California, USA.

0148-0227/09/2009JA014259$09.00

dynamic properties of substorm related phenomena in the ionosphere. Second, the temporal resolution of traditional ISRs is limited by the fact that mechanically shifting of the radar antenna is needed to obtain the physical parameters as a function of latitude/altitude. Unlike the traditional ISRs, the AMISR, with electronic pulse-to-pulse steering capability, allows nearly simultaneous measurement of plasma parameters in multiple look directions without physical movement of the radar antenna [*Heinselman and Nicolls*, 2008]. Therefore, it enables estimation of rapidly evolving convection flows/electric fields in the ionosphere, and is suitable for studying fast evolving substorm processes. Third, PFISR is surrounded by various other types of ground-based instruments. As a part of the NASA Time History of Events and Macroscale Interactions during Substorms (THEMIS) project, 20 Ground-Based Observatories (GBOs), each including an all-sky imager (ASI) and a magnetometer, were deployed over the North America continent, covering more than a quarter of the auroral oval in local time [*Mende et al.*, 2008]. The ASIs provide information about the time, location, and evolution of substorm auroral signatures. In addition, the Alaska magnetometer chain provides magnetic field data along nearly the same geomagnetic meridian as the PFISR radar, which can be used to as a complement and to infer approximately the strength and location of ionospheric currents. A combination of these instruments provides an unprecedented opportunity to study the ionospheric electrodynamics associated with substorms.

[4] The complexity of the substorm process is not only because of its fast temporal evolution, but also because various phenomena associated with substorms occur simultaneously over a vast region of space. In the high latitude ionosphere, substorm related phenomena, such as the substorm current wedge (SCW) and the auroral bulge, often cover a few hrs of MLT. However, the PFISR mode we use allows us to measure plasma parameters along a certain geomagnetic meridian at one time, and as the Earth rotates, measurements are provided along different meridians. In order to obtain a broad 2-D picture from this 1-D measurement, we have divided our events into three categories based on the location of the substorm onset relative to that of the PFISR radar. That is, for different events, PFISR monitored the ionospheric electrodynamics at locations west of, east of, or near the onset meridian. A synthesis of the observations from these three categories then gives us a comprehensive 2-D view of the ionospheric electrodynamics related to substorms.

[5] When the substorm onset occurred east of the radar, we focus on the convection and current changes associated with the westward traveling surge (WTS). The WTS is often observed as the western terminator of the substorm auroral bulge and is associated with the most spectacular and dynamic auroras of the substorm [*Akasofu et al.*, 1965, 1966]. Many different observational techniques and models have been used to study the electrodynamic characteristics of the WTS [e.g., *Inhester et al.*, 1981; *Opgenoorth et al.*, 1983; *Kirkwood et al.*, 1988; *Robinson and Vondrak*, 1990; *Fujii et al.*, 1994; *Hoffman et al.*, 1994; *Marklund et al.*, 1998; *Gjerloev and Hoffman*, 2002]. A common feature revealed by these previous studies is that the WTS is associated with strong upward field-aligned current (FAC) (>2 μA/m^2) and hard electron precipitation (tens of keV) [*Paschmann et al.*, 2002]. An outstanding question regarding the WTS is whether it is closed via the westward auroral electrojet and/or locally distributed meridional Pedersen currents. In the standard SCW picture, the upward FAC of the WTS is closed by the westward auroral electrojet [e.g., *Opgenoorth et al.*, 1983]. However, *Marklund et al.* [1998] indicate that a significant part of the upward FACs is closed by distributed downward FACs through Pedersen currents in the surrounding region. In addition, by using a 3-D current model with empirical conductance and convection electric field models, *Gjerloev and Hoffman* [2002] also found that the meridional Pedersen currents largely contribute to the current closure. In total, we have identified 16 substorms in this category. In section 3.1, we present observations for two of them. Based on all 16 events, we find that westward flows increase equatorward of the WTS and evidence for poleward Pedersen currents flowing toward the WTS and partially closing the upward FAC there.

[6] The evolution of the ionospheric convection east of onset during substorms has received much less attention than that west of onset, perhaps because it is not associated with dynamic aurora as remarkable as the WTS. However, it is the region where downward FACs of the SCW are usually observed [e.g., *Clauer and McPherron*, 1974; *Sergeev et al.*, 1996; *Kamide and Kokubun*, 1996]. *Liang et al.* [2006] utilized four Northern Hemisphere SuperDARN radars and showed that eastward flows in the postmidnight sector increase after onset. For three out of four events, they found that these enhanced flows are the equatorward portion of a newly formed counterclockwise (CCW) vortex, located east and poleward of the auroral brightening region. Recently, also by using the SuperDARN radars, *Miyashita et al.* [2008] found that ionospheric convection of the dawn convection cell began to enhance ~2 min before the onset and persisted throughout the whole expansion phase. In section 3.2, we report PFISR observations of convection changes east of onset for two substorms. Similar to the results of previous studies, an eastward flow channel is found after onset, which we consider in relation to accompanying currents.

[7] When the substorm onset occurs within the field of view (fov) of PFISR, we emphasize the relationship between the breakup arc and the Harang reversal. The Harang reversal, originally named the Harang discontinuity, is the location where the eastward electrojet lies equatorward of the westward electrojet in the same longitudinal plane [*Harang*, 1946; *Heppner*, 1972]. Across the Harang reversal latitudinally, electric fields and thus $\vec{E} \times \vec{B}$ convection flows reverse their direction. The Harang reversal has been proposed to be due to the dawn-dusk pressure asymmetry in the near Earth plasma sheet [*Erickson et al.*, 1991] and therefore, is suggested to be intrinsically a part of the nightside Region 2 current system. This is further confirmed by simulation results from the Rice Convection Model (RCM) [*Gkioulidou et al.*, 2009] using statistical observations from the Geotail spacecraft as boundary conditions, their results emphasizing the necessity of longitudinal overlap between the morning side upward and the evening side downward Region 2 FACs. Note that this overlap of upward and downward FACs in the premidnight sector was also apparent in the original *Iijima and Potemra* [1978] sketch of the Region 1

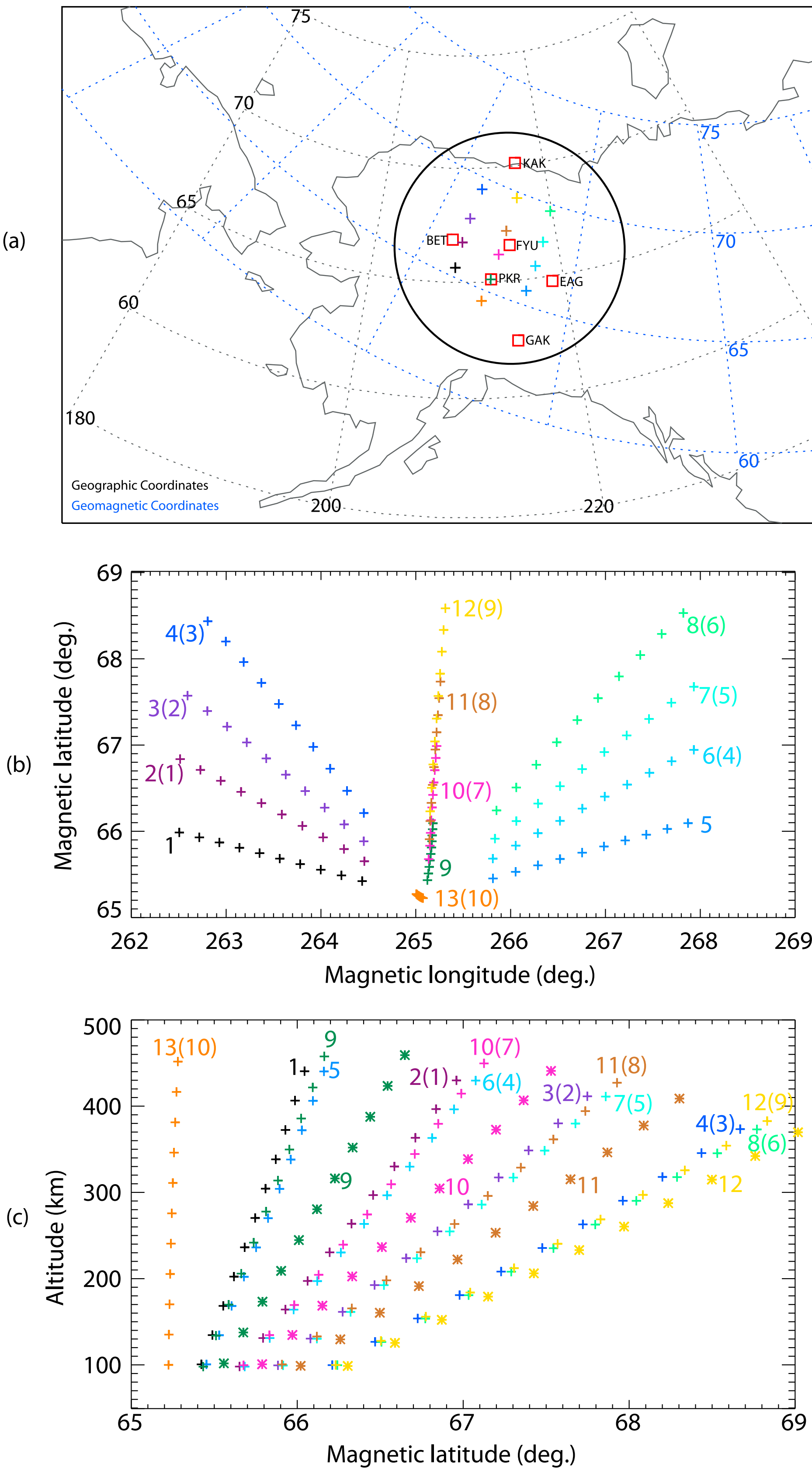
(a)
KAK
BET
FYU
PKR
EAG
GAK
Geographic Coordinates
Geomagnetic Coordinates
(b)
Magnetic latitude (deg.)
Magnetic longitude (deg.)
(c)
Altitude (km)
Magnetic latitude (deg.)

Figure 1

and Region 2 current system, although as stated by the authors, it is not possible to tell whether the upward FAC there belongs to the Region 1 or the Region 2 based on that data set.

[8] The relation between the Harang reversal and the substorm has attracted much attention [*Nielsen and Greenwald*, 1979; *Baumjohann et al.*, 1981; *Robinson et al.*, 1985; *Gjerloev et al.*, 2003; *Bristow et al.*, 2001, 2003; *Bristow and Jensen*, 2007; *Weygand et al.*, 2008; *Zou et al.*, 2009], and the evolution of the reversal have been found to be related to the development of the substorm expansion phase [*Bristow et al.*, 2001, 2003; *Bristow and Jensen*, 2007; *Zou et al.*, 2009]. Mainly due to instrument limitations, the location of the Harang reversal to that of substorm onset has not yet been clarified. Recently, *Zou et al.* [2009] used observations from the TIGER radar pair in the Southern Hemisphere and the IMAGE WIC camera and showed clearly that the several substorm onsets they studied occurred in the center of the Harang reversal.

[9] However, the initial breakup arc of a substorm onset is often too thin (a couple of or even tenths of kilometers) [e.g., *Borovsky*, 1993, and reference therein] to be revealed by global auroral images from high-altitude satellites. The THEMIS ASI is able to detect the initial breakup arc with its high spatial resolution, especially at zenith where the resolution can be as high as ~1 km [*Donovan et al.*, 2006]. In addition, the SuperDARN data presented by *Zou et al.* [2009] had been mapped to a global grid and the latitudinal resolution is ~110 km (~1°), whereas the PFISR radar used here has approximately twice this latitudinal resolution. Therefore, in this paper, we utilize the PFISR and THEMIS ASIs observations to study the relationship between the Harang reversal and the breakup arc. Observations of two substorm events for which the breakup arc occurred near the center of the PFISR fov are presented in section 3.3. The relation of the breakup arc to the location and evolution of the Harang reversal in the premidnight sector is discussed.

[10] In the following section, we present details of PFISR and the THEMIS ASIs. We then describe multi-instrument observations of six substorm events, two for each category. Last, we synthesize the observations and draw conclusions from them.

2. Instrumentation

[11] Figure 1a shows the fov of the PFISR radar with the 13-beam configuration used in our studies in geographic (black) coordinates. Each plus sign represents the geographic location of one radar beam at ~550 km altitude. Geomagnetic coordinates (blue) are further superposed. The large circle represents the fov of the ASI at Fort Yukon (FYKN), which fully covers the fov of PFISR. Red squares indicate the locations of six magnetometers of the Alaska chain. Between March 2007 and October 2008, ~90 runs were conducted when PFISR was on the nightside, extending from ~19 (0610) MLT (UT) to ~4 (1510) MLT (UT). The runs before June 2007 used a 10-beam mode and those after used the 13-beam mode.

[12] In Figures 1b and 1c, the radar beams, with beam number indicated, are projected onto geomagnetic horizontal and meridional planes, respectively. Different beams are color-coded for clarification and beam numbers in parentheses are of the 10-beam configuration. The 13(10)-beam radar configuration includes beams 1–4(1–3) pointing to the northwest, beams 5–8(4–6) to the northeast, beams 9–12(7–9) directly to the north, and beam 13(10) up along the magnetic field. These beam configurations are designed to simultaneously obtain data with the largest magnetic latitude coverage and with the highest temporal resolution.

[13] During these experiments, two types of pulses were transmitted, a long pulse (~72 km range resolution) and an alternating code pulse (~4.5 km range resolution). The former is appropriate for *F* region measurements and the latter for the E region. Los ion velocity measurements from all beams are used to calculate the convection vectors under the assumption that the velocity vectors are homogeneous in the east-west direction across the radar fov. The appropriate component of the parallel velocities measured by beam 13(10) are subtracted during the calculation. The central beams 9–12(7–9) of the 13(10)-beam mode provide electron density profiles as a function of altitude/latitude along the same geomagnetic meridian. More information about the radar transmission schemes and the methodology of resolving vector velocities can be found in the work of *Heinselman and Nicolls* [2008].

[14] The THEMIS ASIs are white light CCD imagers. Each of them has latitudinal coverage of ~9° and longitude coverage of slightly more than one hr MLT. They are able to image aurora with high temporal (3 s exposure cadence) and spatial resolutions [*Mende et al.*, 2008]. All the auroral images presented in this paper are under the assumption of a 110 km emission height.

3. Multicase Study

[15] Here we present two typical examples for each of the three categories of substorm onset location relative to the PFISR location.

3.1. Substorm Onset East of PFISR

[16] Two substorm events are presented with the first onset located east of, but very close to, PFISR and the other located further to the east. In both cases, the prevailing ionospheric convection flows were in the westward direction. Assuming the electrojet is mainly composed of Hall

Figure 1. (a) PFISR field of view of 13-beam mode is shown in geographic (black) coordinates. Each plus sign represents the location of one radar beam at ~550 km in altitude. Geomagnetic coordinates (blue) are also superposed onto the plot, and the geomagnetic longitude lines are 1 h apart starting from the Churchill meridian. Field of view of ASI at Fort Yukon (circle) and locations of six ground-based magnetometers (squares) are also shown. (b) Projection of PFISR 13(10)-beam mode configuration in geomagnetic coordinates. (c) Projection of PFISR 13(10)-beam mode configuration in geomagnetic meridional plane. Since 30 November 2007, the pointing directions for beams 9–12 have been changed, as shown by asterisks in Figure 1c, for the purpose of increasing the latitudinal coverage of electron density measurement.

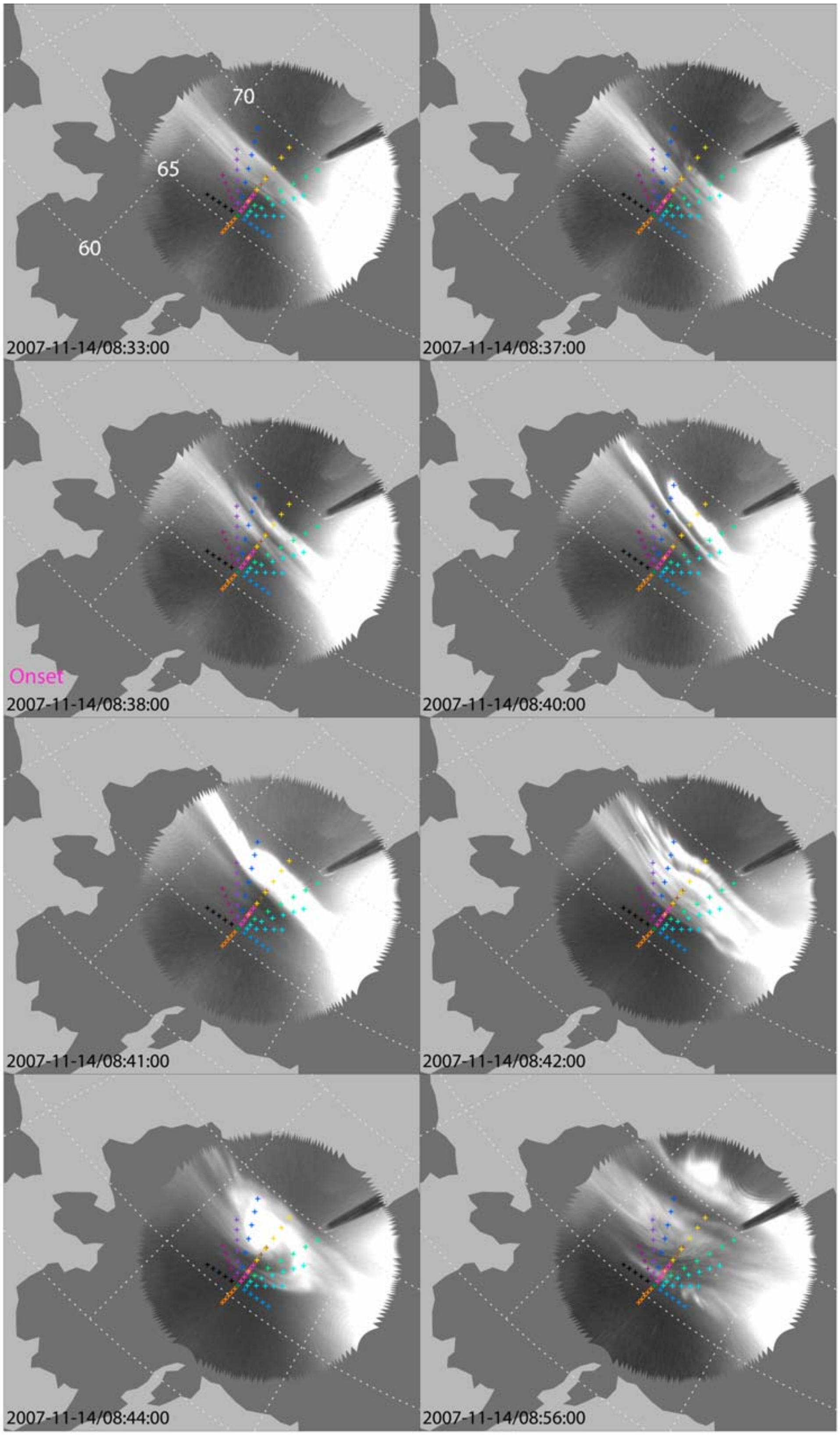

Figure 2. Selected auroral images obtained by the ASI at Fort Yukon on 14 November 2007, with PFISR beams projected. Geomagnetic coordinates are also shown as white dotted lines. The substorm onset was at ~0838 UT. The PFISR radar was located at ~21.6 MLT around this time.

current, this means PFISR was monitoring the eastward auroral electrojet region.

[17] The first event occurred on 14 November 2007. Figure 2 displays eight selected auroral images taken by the imager located at FYKN from the growth phase to the recovery phase. Geomagnetic coordinates and the locations of the PFISR radar beams are projected onto each image. The universal time (UT) when the image was taken is indicated at the lower left corner of each image. In the first image, an east-west-extending diffuse aurora band can be seen in the center of the image, with width wider than 1° in latitude. Note that the broad region of apparent brightness in the easternmost portion of the image is contamination due to the moon. The following image shows a dimming in the poleward portion of this diffuse aurora band along and to the west of the center meridian of PFISR. There is also evidence for some brightening to the east in this image. At 0838 UT, a clear discrete arc can be seen which extended from this brightening to the location of the aurora dimming. In the later images, this discrete arc bifurcated, brightened further and expanded poleward and westward. By 0844 UT, a very well defined auroral spiral, which is a typical signature of the WTS, was apparent within the radar fov but slightly to the west of its center meridian. The aurora continued to expand and at 0849 UT, its equatorward portion reached well into the *E* region radar fov.

[18] Observations from PFISR and Alaska magnetometers from 08 to 10 UT are synthesized and shown in Figure 3. Figure 3 shows the convection flow direction (Figure 3a), magnitude (Figure 3b), and vector (Figure 3c), the raw electron density profiles from beams 12 (Figure 3d), 10 (Figure 3e), and 13 (Figure 3f), as well as the H, D, and Z components of the ground magnetic perturbations recorded by four of the Alaska magnetometers (Figure 3g). The magenta line indicates the time of onset determined by the auroral signature. The onset might have been 2 min earlier based on the magnetic perturbation at Poker Flat. The convection flow data here were processed at ~3 min time resolution and were binned into 0.5° mlat bins every 0.25°, while the electron density is shown with ~1 min time resolution. Details of the Figure 3 format are described in the caption.

[19] As shown in Figures 3b and 3c, westward flows within the equatorward portion of the PFISR fov (which may have extended to lower latitude, but out of the radar fov) suddenly enhanced at ~0842 UT and persisted for about 10 min. The peak flow speed reached 1000 m/s (~50 mV/m), when the auroral spiral developed poleward of the enhanced flows. At 0852 UT, the strong flows significantly decreased to ~500 m/s and then maintained that level until ~0930 UT, which marked the end of the recovery phase. The enhanced westward flows between ~0842 UT and 0852 UT show a clear equatorward gradient, which indicates converging poleward electric fields and thus suggests converging poleward directed Pedersen currents. These converging Pedersen currents are anticipated to be associated with upward FACs.

[20] Indeed, simultaneous ionization profiles observed by beam 10 and beam 12 show enhancement of ionization at ~65.7° to 66.5° mlat, indicating an enhancement of energized electron precipitation and this of upward FAC. The peak ionization was seen at ~66.23° mlat at 0850 UT, roughly where the strongest velocity gradient was located. By further combining the auroral image and the ionization observations, it is clear that this ionization enhancement and inferred upward FAC were associated with the equatorward portion of the auroral spiral and its later expansion. In contrast, beam 13, which is located at the lowest latitude and upward along the magnetic field, did not record an obvious enhancement of ionization from that of a preexisting, relatively steady ionization band.

[21] The westward flow enhancement also suggests an enhancement of the eastward electrojet. In Figure 3g, significant ground magnetic perturbations can be seen, with the strongest perturbations at the three highest latitude magnetometers occurring at the same time as the flow and ionization peaks. The positive H perturbation recorded by all but the highest latitude station indicates intensification of the eastward electrojet, as have been reported by *Rostoker and Kisabeth* [1973]. This eastward electrojet is likely associated with the observed flow enhancements, at least at the two lower latitude stations, which are located equatorward of the region of ionization enhancement. The reversal of sign in the H perturbations between Fort Yukon (~67.3° mlat) and the highest latitude station Kaktovik (~71.1° mlat) indicates that the magnetic Harang reversal, i.e., ΔH = 0, was located between these two stations during the expansion phase.

[22] The flow and ionization observations described here suggest that the poleward Petersen currents contributed at least partially to the local closure of the upward FAC associated with the WTS, consistent with low-altitude polar-orbiting satellite observations [*Marklund et al.*, 1998]. However, due to the narrow latitudinal fov of the radar, the lower latitude portion of the enhanced westward flows cannot be observed. However, as shown in Figures 2

Figure 3. (a–c) Nightside convection flow direction, magnitude, and vector measured by PFISR on 14 November 2007 are shown as a function of magnetic latitude and universal time; data are plotted only if the measurement uncertainty is less than 200 m/s. In Figure 3a, the direction of the flow is zero if pointing to the magnetic north and increases (decreases) clockwise (counterclockwise). In Figure 3c, flows with eastward component are blue, and those with westward component are red. (d–f) Raw electron densities with no correction for T_e/T_i or Debye length effects measured by beam 12, 10, and 13 (upward along magnetic field) are shown as a function of universal time. Altitude is indicated on the left Y axis and magnetic latitude is indicated on the right Y axis. Electron density below 175 km is from the alternating code pulse measurement, while that above 175 km is from the long pulse measurement. (g) Magnetic perturbations of H (red), D (blue) and Z (green) components recorded by four Alaska magnetometers that are roughly at the same local time are shown as a function of universal time. The value of each component at the beginning of this period is subtracted and represented by a horizontal dashed line. The name and geomagnetic location of each magnetometer are shown to the left. The vertical magenta line indicates the substorm onset time based on auroral images.

and 3g, Gakona (∼63.1°) was located within the low auroral luminosity region but recorded positive H perturbation, which implies that westward flows increased and that the enhanced flows extended equatorward of the radar fov. While a quantitative calculation of the Pedersen current convergence would require calculation of ionospheric conductivities versus latitude, which is beyond the scope of this paper, the existence of the magnetic Harang reversal

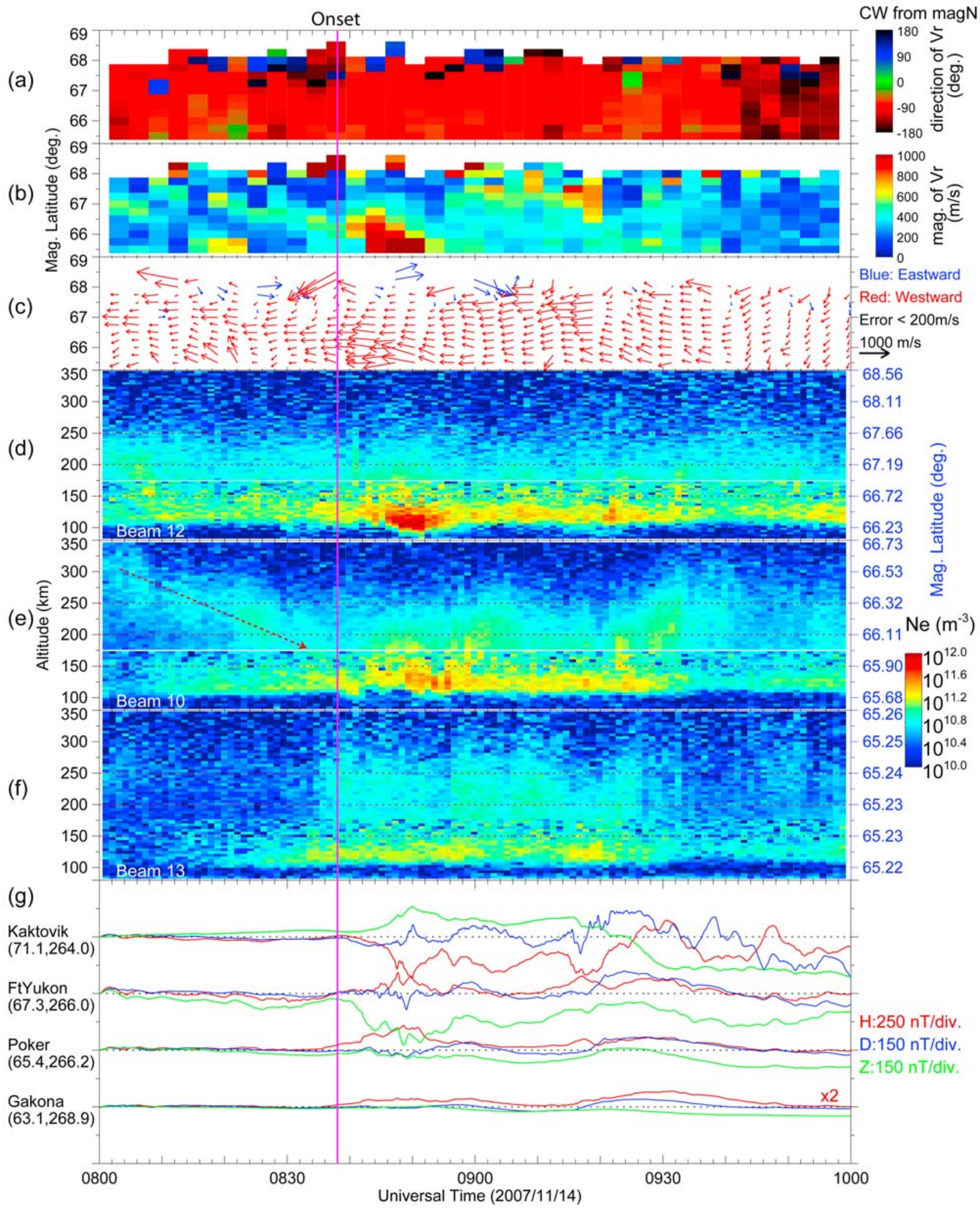

Figure 3

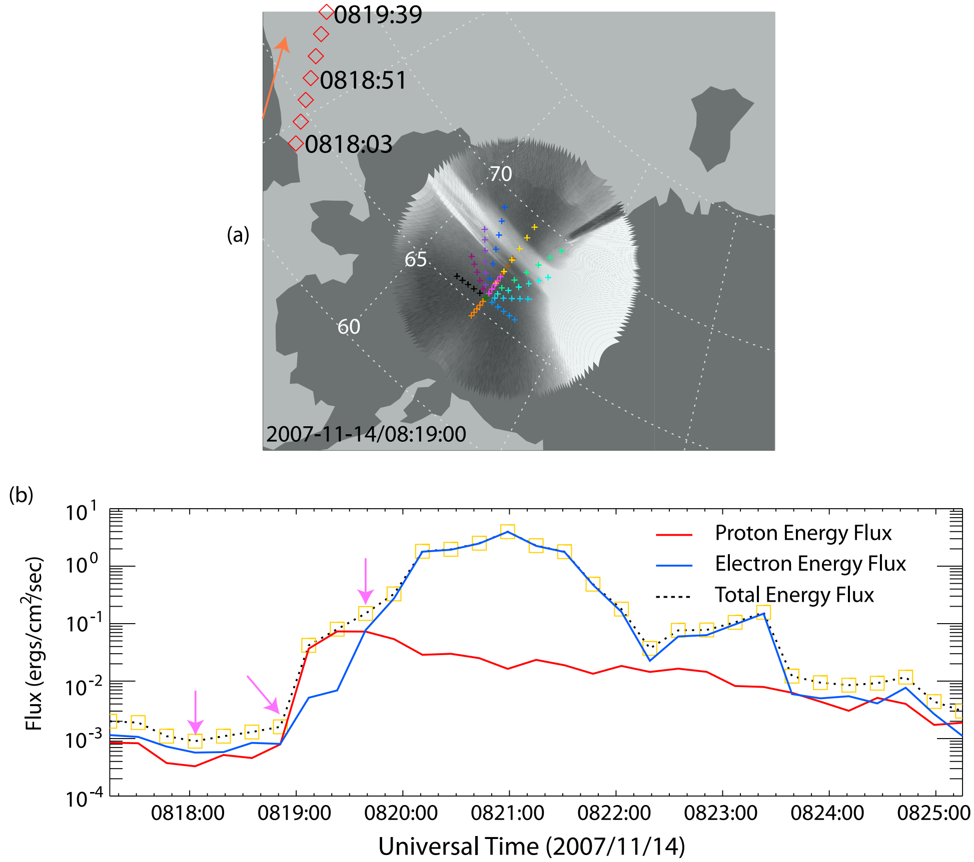

Figure 4. (a) Auroral image taken by the ASI at Fort Yukon at 0819 UT. The PFISR radar was located at ~21.2 MLT at this time. Red open diamond represents the footprint of the satellite every 16 s starting at 0818:03 UT. (b) The NOAA-17 satellite observations of the total energy fluxes carried by precipitating electrons (blue curve), by protons (red curve), and by both of them (dotted black curve). The particle energies range from 50 eV to 20 keV.

indicates that the enhanced poleward Pedersen current equatorward of the surge must be diverted upward equatorward or at the reversal, consistent with our inference that these currents contribute to the upward FAC of the WTS.

[23] The westward flow/poleward electric field enhancement observed here is similar to the SuperDARN observations described by *Zou et al.* [2009]. In the work of Zou et al., a sudden increase in westward flows was observed at onset just equatorward of the onset brightening, while in this case delay was observed probably because the radar was slightly west of the onset. Zou et al. also found that the majority of the enhanced westward flows at onset were Sub-Auroral Polarization Streams (SAPS). SAPS represent westward flows in a broad, low conductivity region predominantly in the premidnight sector with peak flows equatorward of the auroral electron precipitation [*Foster and Burke*, 2002, and references therein]. SAPS are usually found to be collocated with the downward Region 2 FACs and its equatorward extent is coincident with the ion precipitation [*Anderson et al.*, 1993, 2001], and their generation is a manifestation of magnetosphere-ionosphere coupling related with the Region 2 FAC system [*Anderson et al.*, 1993; *Foster and Burke*, 2002]. Thus the question arises as to whether the enhanced westward flows observed by PFISR were also in the subauroral region.

[24] In Figure 3e, during the growth phase, two bands of electron density enhancements are apparent. The upper band, highlighted by a red dashed arrow, gradually moved to lower latitude/altitude, while the lower band was almost homogeneous and confined between ~100 km and 150 km in the E region. At the end of the growth phase, the two bands joined together. A similar *E* region ionization band can also be seen in beam 13, which initiated several minutes later than that in beam 10. This indicates that the source of these ionization features gradually moved earthward in the plasma sheet during the growth phase. This homogeneous ionization band lasted until ~0930 UT. At higher altitudes, beam 13 started to observe weak ionization enhancement in the F region around onset, which should be due to soft (<1 keV) electron precipitation [*Rees*, 1963] associated with the earthward movement of the inner edge of the electron plasma sheet at onset.

[25] Energetic particles pitch angle scattered from the plasma sheet are believed to be the major source of the *E* region ionization in the nighttime. In the evening sector, energetic protons have been shown to be an important source of the *E* region ionization near the equatorward edge of the electron precipitation [*Robinson and Vondrak*, 1985; *Senior et al.*, 1987] and the Pedersen and Hall conductances produced by protons have been parameterized by *Galand and Richmond* [2001]. By using the Chatanika ISR and

polar-orbiting satellites measurements, *Robinson and Vondrak* [1985] found that, at times, the *E* region ionization may be almost entirely due to precipitating protons. The relative contribution of the precipitating electrons and protons to the *E* region ionization has been calculated by *Lilensten and Galand* [1998] and *Smirnova et al.* [2004] for a coordinated DMSP/EISCAT experiment [*Anderson et al.*, 1997] where the proton energy flux was a couple times higher than the electron energy flux. Both of these studies found that proton precipitation gives a far more prominent ionization peak in the E region (<150 km) and decreases significantly below ~100 km. In Figures 3e and 3f, the ionization of the lower band during the growth phase was confined between ~100 km and ~150 km, suggesting that the source of the ionization is precipitating protons. Its distinction from the equatorward moving region of soft electron precipitation observed by beam 10 (Figure 3e) is consistent with this interpretation.

[26] In the present case, fortuitously, during the growth phase and when the continuous *E* region ionization was observed, the NOAA-17 satellite moved from low latitude to the polar region ~1.5 h of MLT west of PFISR. Figure 4a shows the auroral image taken at 0819 UT. Red open square represents the footprint of the satellite every 16 s. The starting and the ending times of the squares, together with the time when the total energy flux of protons started to exceed that of electrons are indicated next to the appropriate squares. Figure 4b shows the total energy fluxes carried by protons (red curve), by electrons (blue curve), and by both of them (black dotted curve) as a function of UT. The particle energies range from 50 eV to 20 keV. The three arrows point to the fluxes for the UTs marked in Figure 4a. As can be seen, the proton energy flux exceeded the electron energy flux between 0818:51 UT, when NOAA-17 was at ~66° mlat, and 0819:39 UT, when it was at ~68° mlat,. At the time when the proton energy flux reached its peak, it contributed more than 90% of the total energy flux. Therefore, they played a dominant role in ionization the E region and contributed significantly to the conductivity in this region. Considering the fact that the equatorward boundary of the proton precipitation gradually moves to lower latitudes at later local times, this observation suggests that beam 10 (magenta) was embedded within the enhanced proton precipitation region. Later, this region extended further equatorward and engulfed beam 13 (orange). These satellite observations further support our suggestion that the homogenous *E* region ionization enhancement during the growth phase is due to energetic proton precipitation. Similar continuous *E* region ionization due to precipitating protons is frequently observed by PFISR in the premidnight sector and this example is typical of what is observed.

[27] It seems plausible that the upper band of electron density enhancement in Figure 3e is due to soft precipitating electrons. However, we cannot distinguish whether its slow movement to lower altitude/latitude is a temporal and/or a spatial effect. If the former is true, it may be related to gradual energization and earthward motion of the electron plasma sheet during the growth phase and if the latter is the case, it suggests the electron plasma sheet is closer to the Earth at later MLT. It could also be an effect of both.

[28] The above observations indicate that the enhanced westward flows seen between ~0842 UT and 0852 UT were located in a region that was equatorward of the electron precipitation boundary and embedded within almost pure proton precipitation during the growth phase, and were engulfed by the equatorward expansion of the electron precipitation boundary after onset. Note that as shown in Figure 2, beam 13 was always embedded in low auroral luminosity region. Thus the enhanced westward flows observed by PFISR are the poleward portion of SAPS, which probably extended further equatorward as suggested by the Gakona magnetometer observations.

[29] The second substorm of this category was on 5 May 2008. Figure 5a displays selected auroral images taken by the ASI located at Fort Simpson (FSIM), and Figure 5b shows ground magnetic perturbations recorded by three THEMIS ground-based magnetometers located at about the same latitude but roughly 1 h MLT apart from each other. Although the full picture of the auroral onset was not captured by the THEMIS ASIs east of FSIM because of cloudy skies, the western edge of the onset arc can still be seen in the east portion of the FSIM ASI at 0650 UT. This onset arc appeared just poleward of a diffuse aurora band near 65° mlat. At ~0654 UT, a typical aurora WTS became very well defined within the ASI fov. Another obvious auroral brightening can be seen near the western edge of the ASI fov at 0647 UT, which appeared to be a pseudo breakup because of a lack of poleward expansion.

[30] In Figure 5b, the magnetic perturbations associated with the onset is first seen at Gillam (GILL) at ~0650 UT, the same time as the brightening in the FSIM ASI. By combining the auroral and ground magnetic signatures together, it is clear that the onset occurred at ~0650 UT and was located east of the FSIM ASI and near GILL. In Figure 5b, a positive spike in the D component was recorded by both FSIM and Fort Smith (FSMI) stations, with a couple minutes delay at FSIM, indicating a westward propagation of the WTS head. Comparing the timing of the spike with the optical observations, we found that the head of the WTS swept over FSIM at the time of the D component spike, consistent with results presented by *Tighe and Rostoker* [1981].

[31] Figure 6 shows the PFISR radar and ground-based magnetometer observations during this period in the same format as Figure 3. Enhanced ionization initiated several minutes after the onset but without significant magnetic perturbation. Figure 6g shows prominent positive D perturbations at all stations indicating passage of the WTS. In addition, the D perturbation was seen first at the lowest latitude station (at ~0710 UT) and then moved to higher latitudes, implying a poleward motion of the WTS. As shown in Figures 6b and 6c, simultaneously with the large positive D perturbation from ~0716 to ~0726 UT was an increase in the westward flows, identified in Figure 6 by a fuchsia arrow. The peak flow speed exceeded 1000 m/s and the flow enhancement lasted for about 15 min. In Figure 6d, the peak *E* region ionization enhancement occurred at 0718 UT and at ~66.4° mlat, near the strongest flow gradient. This flow-ionization relation is quite similar to that during the previous event and also suggests a partial closure of the upward FAC in the WTS by the poleward directed Pedersen currents.

[32] During the 90 radar runs, 16 substorm events fall into this category, 12 of them having concurrent ASI observa-

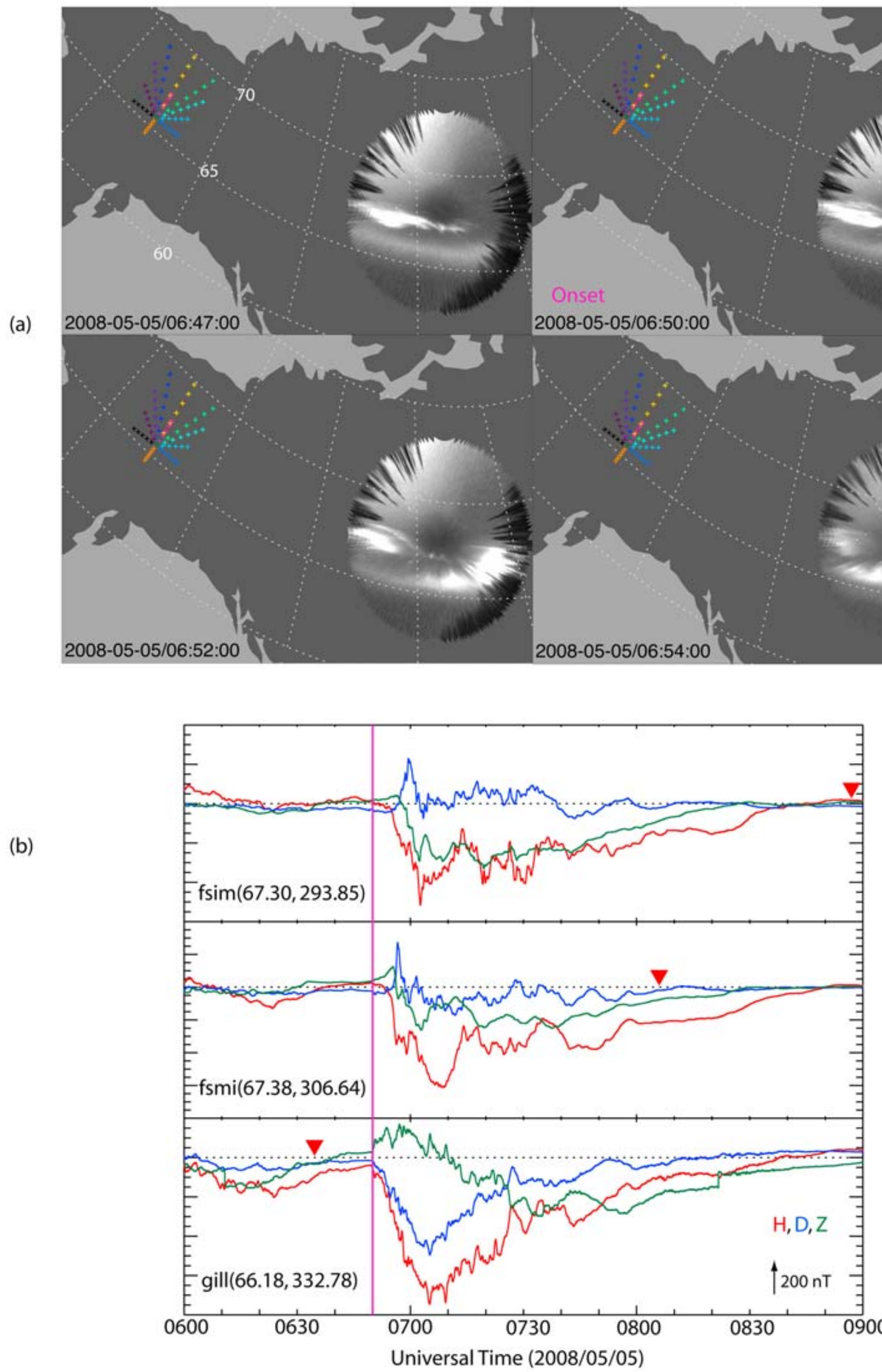

Figure 5. (a) Selected auroral images observed by the ASI at Fort Smith on 5 May 2008, with PFISR beams projected. The PFISR radar was located at ∼19.7 MLT at 0650 UT. (b) Magnetic perturbations of H (red), D (blue), and Z (green) components recorded by three THEMIS GBO magnetometers are shown as a function of universal time. The average of each component during this period is subtracted and represented by the horizontal dashed line. Red triangle represents the magnetic local time in universal time for each station. The vertical magenta line indicates the substorm onset time based on auroral images. The substorm onset was at ∼0650 UT and near Gillam.

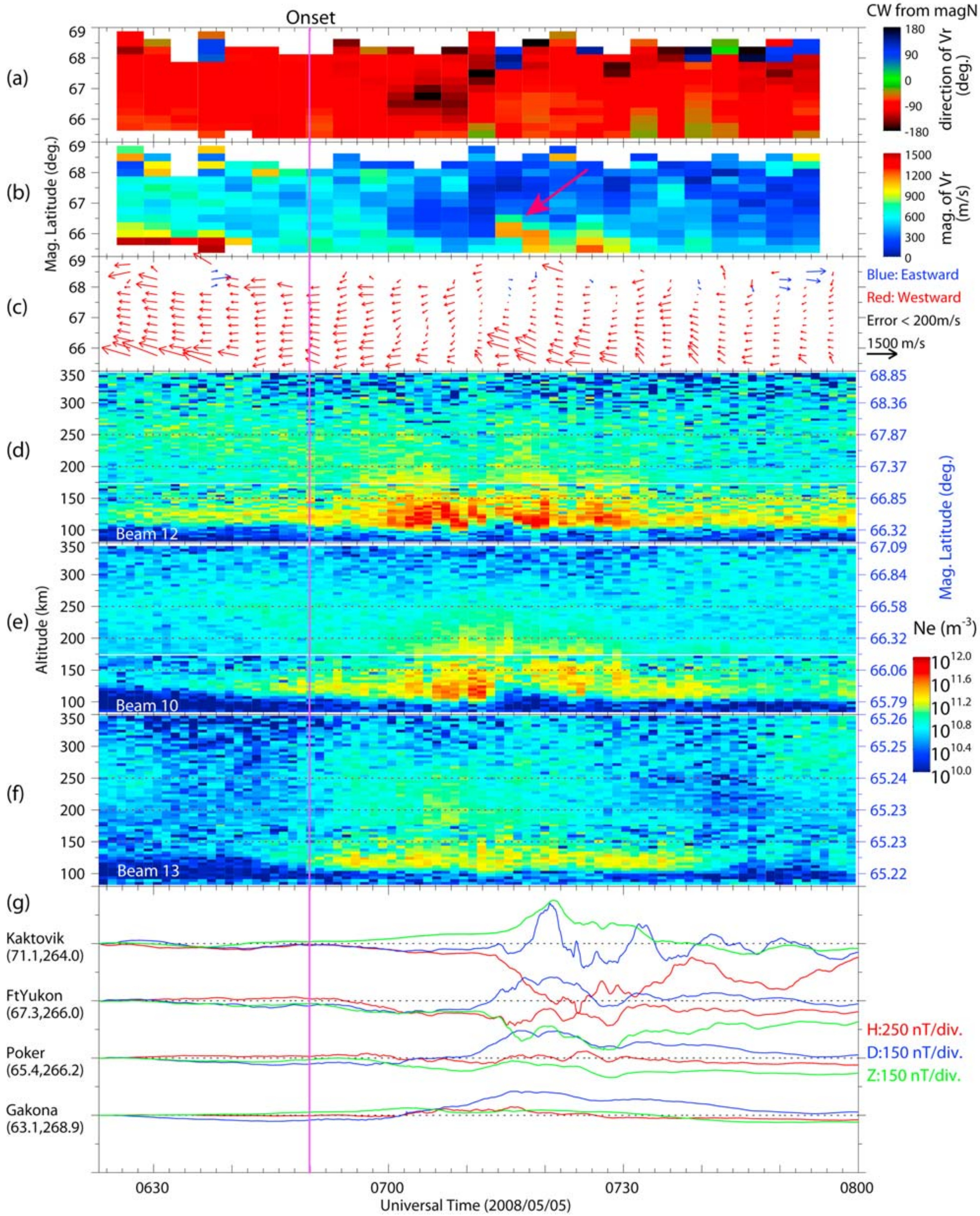

Figure 6. Same as Figure 3 but for the substorm at ~0650 UT on 5 May 2008.

tions and the other 4 events being inferred from the positive D perturbation associated with the WTS recorded by ground-based magnetometers. All of these events show a repeating signature. That is westward flows/poleward electric fields increase in response to the passage of the WTS poleward of them. This is consistent with poleward Pedersen currents associated with these westward flows contributing at least partially to the closure of the upward FAC in the WTS region. For several events, the location of the WTS was well poleward of the *E* region PFISR fov. These events

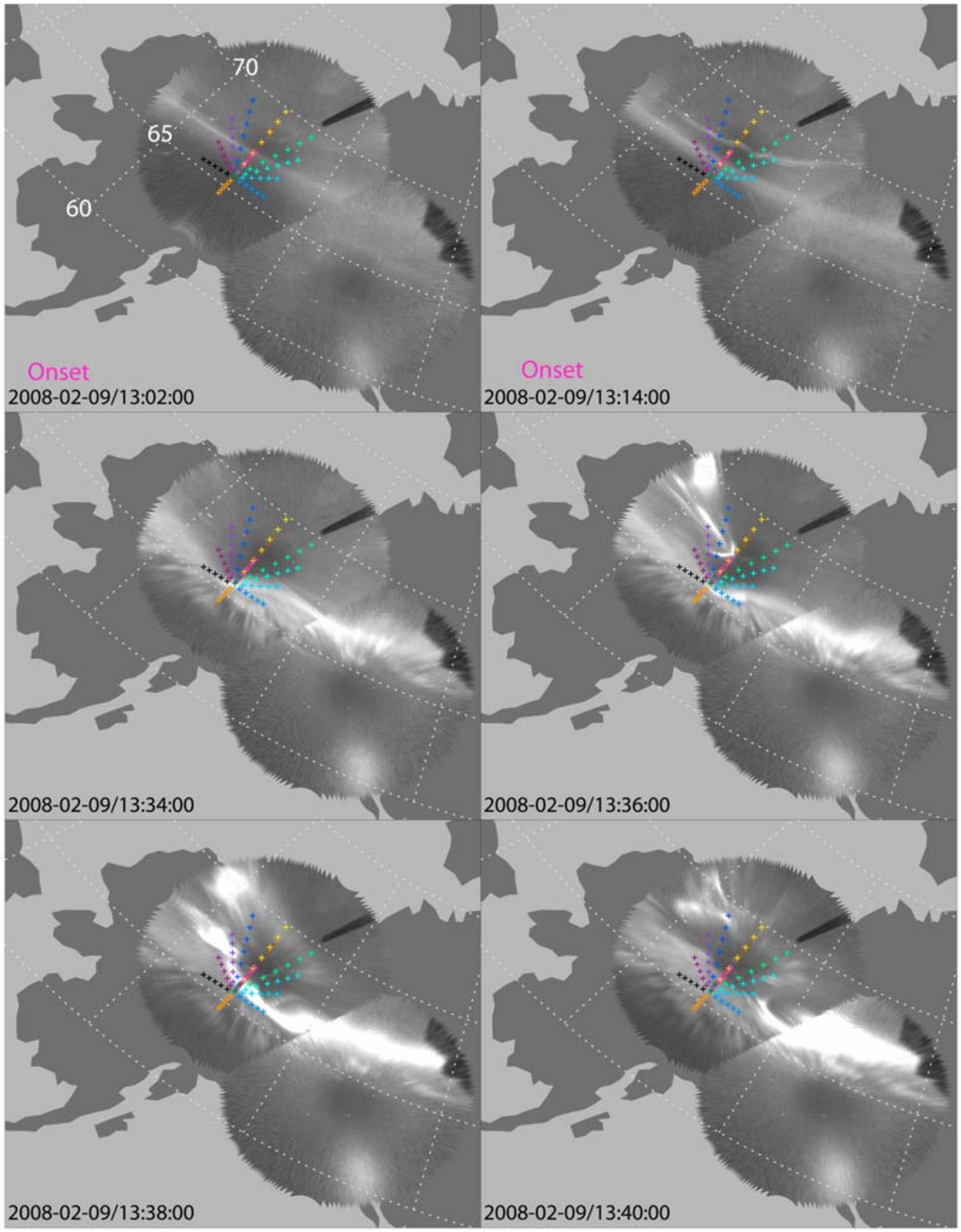

Figure 7. Selected auroral images observed by the ASIs at Fort Yukon and at White on 9 February 2008. The PFISR radar was located at ∼1.97 MLT at 1302 UT in the postmidnight sector.

allowed us to observe that the enhanced westward flows extend well into the subauroral region.

3.2. Substorm Onset West of PFISR

[33] In this section, we present two substorm events having auroral onsets located west of the PFISR radar. In both cases, the PFISR radar was in the postmidnight sector and the prevailing ionospheric convection flows were in the eastward direction. Thus PFISR was monitoring the westward aurora electrojet region.

[34] On 9 February 2008, two consecutive substorms were observed by the POLAR UVI over the Southern Hemisphere (not shown). The first onset occurred near 22 MLT at ∼1301:49 UT and the second one initiated slightly to the east near magnetic midnight at ∼1315:19 UT. Both onsets occurred far to the west of PFISR, which was near ∼2 MLT in the post midnight sector at the time of onset. Images taken after both onsets show poleward and azimuthal expansions, and thus formation of an auroral bulge. By ∼1336 UT, the eastern edge of the auroral bulge moved to ∼2.5 MLT, roughly where PFISR was located at that time.

[35] Figure 7 shows selected auroral images taken by the ASIs at FYKN and White (WHIT) at and after the substorm onsets. Since both onsets were far to the west, no brightening of discrete aurora arc was seen by these ASIs at the onset times. After the onset, diffuse aurora gradually

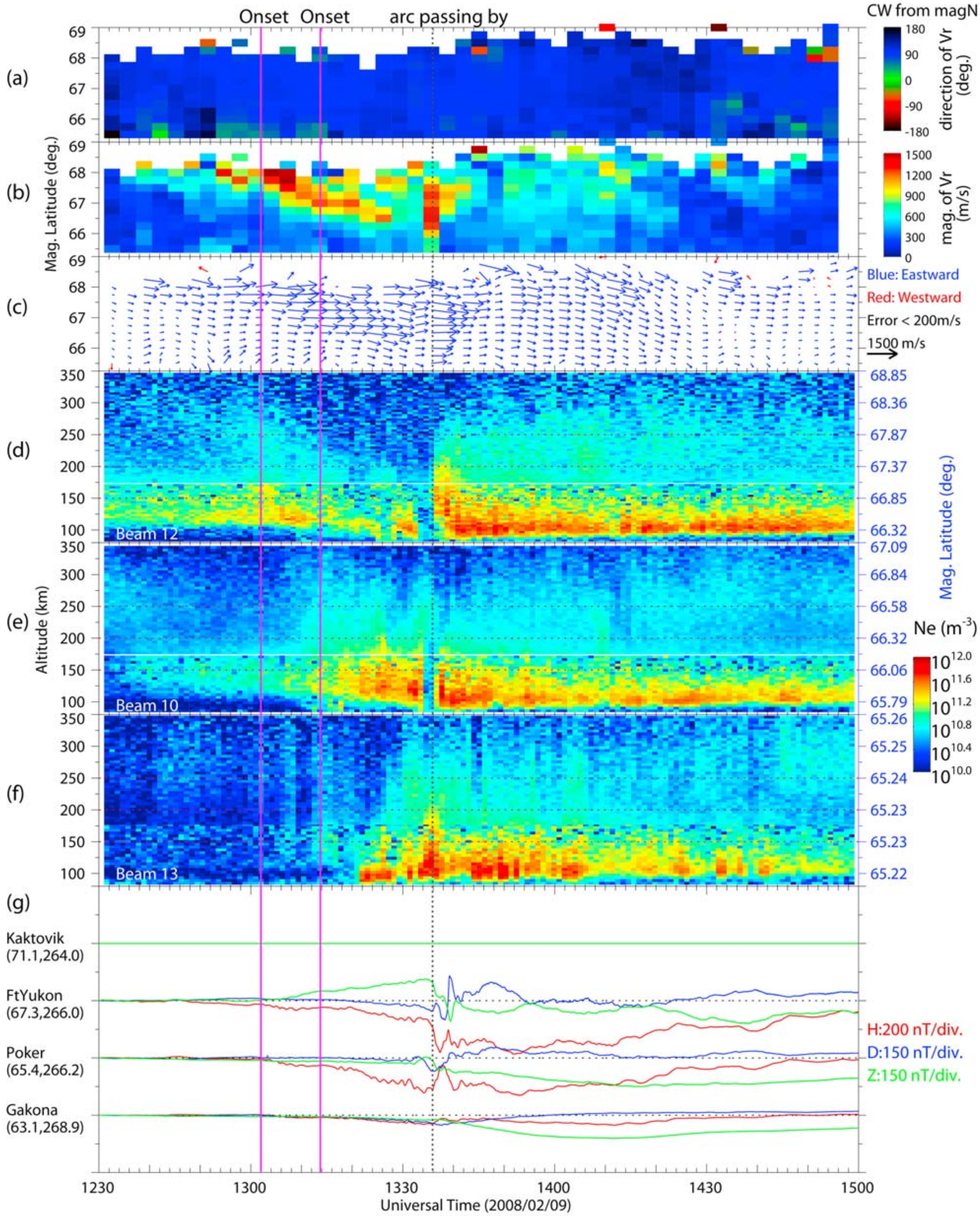

Figure 8. Same as Figure 3 but for the substorms at ~1302 and ~1314 UT on 9 February 2008.

enhanced equatorward of ~66° mlat and moved equatorward. At 1336 UT, a bright auroral form propagated into the FYKN ASI from the west, indicating the eastward expansion of the auroral bulge and consistent with the POLAR observations.

[36] Figure 8 shows the PFISR and ground magnetometer observations from 1230 to 1500 UT of this day, in the same format as Figure 3. Two magenta lines indicate the onset times determined by the POLAR UVI observations, and the black dashed line indicates the time when the bright aurora

arc intruded into the PFISR fov. In Figures 8b and 8c, an eastward flow enhancement can be seen at the poleward portion of the PFISR fov which initiated before the first onset, similar to the SuperDARN observations reported by *Zou et al.* [2009]. As shown in Figure 8d, before the first onset, weakly enhanced ionization was observed by beam 12 which extended up to ~200 km. The concurrent ASI observations show weak diffuse aurora poleward of beam 13. Based on statistical and simulation results, this region is anticipated to be part of the Region 2 upward FAC area [*Iijima and Potemra*, 1978; *Gkioulidou et al.*, 2009]. The first two aurora images in Figure 7 indeed confirm that there were weak east-west-extending aurora bands near 66° mlat composed of probably both diffuse and discrete auroras.

[37] After the first onset, these eastward flows were further enhanced and gradually moved to lower latitude. During the expansion phase of the second substorm, an enhanced flow channel with poleward gradient at lower latitude and equatorward gradient at higher latitude formed and protruded into the radar *E* region fov. In Figure 8d, depletion in the *E* region ionization was captured by beam 12 after the second onset. The depletion was located approximately at and poleward of the peak of the enhanced eastward flows and within the inferred previous upward Region 2 FAC regime. Because the radar fov is limited, the *E* region electron density profile is not available poleward of 66.85° mlat. Nevertheless, a lack of brightening aurora poleward of ~67° mlat at 1334 UT in Figure 7 suggests that reduced *E* region conductivity may have extended further poleward of the *E* region radar fov. In contrast, there was a significant increase in the *E* region ionization after the second onset in beams 10 and 13, just equatorward of the peak enhanced flows. The ionization increase was slightly delayed in beam 13 implying equatorward propagation of the precipitation source. The ASI observations shown in Figure 7 suggests that the ionization enhancement was due to intense and equatorward moving diffuse aurora. The density depletion was not observed for the first onset, because the eastward flow enhancement occurred at higher latitude so that only the poleward velocity gradient and the associated density enhancement were captured by the radar *E* region fov.

[38] As suggested by Figure 8b, there are equatorward and poleward velocity gradients at latitudes higher and lower, respectively, than the peak of the enhanced flows. At lower latitude, the poleward velocity gradient indicates a poleward gradient of the equatorward pointing electric field and thus converging equatorward flowing Pedersen currents. This, together with the observed enhanced ionization there, suggests existence of enhanced upward FACs. On the other hand, at higher latitude, the equatorward velocity gradient indicates diverging electric fields and thus diverging Pedersen currents. Along with the observation of density depletion, the observation suggests a formation of downward FAC. In addition, the ionization reduction started right after the second onset, suggesting that this downward FAC formed at onset and should belong to the SCW system. The formation of downward FAC east of the auroral bulge is consistent with the classical picture of the SCW system [e.g., *Sergeev et al.*, 1996]. The above observations indicate that the downward FACs formed at onset were at least partially closed by the upward FACs equatorward of it.

[39] After 1336 UT when the bright arc intruded into the PFISR fov, intense ionization appeared in beam 12. Elongated ionization probably caused by broadband electron precipitation were seen for a couple of minutes and followed by more energetic electron precipitation that penetrated to an altitude of ~90 km. (Note that plasma sheet protons, such as those that can be seen in Figure 3e, do not penetrate below ~100 km, as also noted by *Robinson and Vondrak* [1985].) As the ionization increased, the large eastward flows decreased to ~600 m/s and lasted for more than half an hour. The flow directions show some modest and gradual rotation from almost purely eastward to southeastward.

[40] During the period shown in Figure 8, the convection flows were mainly in the eastward direction, which implies that the Alaska magnetometer chain was under the influence of westward electrojet. Indeed, in Figure 8g, all the stations (no data for Kaktovik station) recorded negative H perturbation. Transient and large magnetic perturbations were associated with the intrusion of the aurora at ~1336 UT. A bipolar signature in the D component can be seen clearly at Fort Yukon and less clearer at Poker Flat. In the H component, there are a local minimum and a local maximum recorded by Fort Yukon and Poker Flat, respectively. These signatures can be well explained by assuming a counter clockwise vortex of Hall current associated with an upward FAC. Over a larger time scale, the negative H bay observed by magnetometers at Fort Yukon and Poker Flat significantly increased after the auroral intrusion, indicating strengthening of the westward auroral electrojet overhead. Another noticeable feature is the variation in the Z component at Fort Yukon. After the sweep of the auroral bulge, the sign of the perturbation changed from positive to negative, which indicates a poleward shift of the center of the westward electrojet. Therefore, although the electric field decreased, the westward electrojet still increased at higher latitude due to increase of the Hall conductivity and the peak current moved to higher latitude.

[41] Figures 9 and 10 show an auroral image sequence from the FYKN ASI and PFISR observations of a substorm on 13 February 2008, that are quite similar to Figures 7 and 8. The first substorm onset signature was captured by the THEMIS A spacecraft in the premidnight sector near ~1337 UT, when PFISR was ~2.5 MLT. Therefore, the optical onset should occur to the west of PFISR, although we could not determine its exact location. In Figure 10b, similar to the previous event, eastward flows within the poleward portion of the PFISR fov were enhanced slightly during the growth phase. The weakly enhanced ionization up to ~200 km observed by beam 12 and beam 10 initiated roughly the same time as the flow enhancement and suggests the existence of weak upward FAC due to converging Pedersen currents. The concurrent ASI observations indicate that the radar *E* region fov was indeed embedded within a diffuse aurora band.

[42] After the onset, the eastward flows increased substantially, with peak velocity exceeding 1600 m/s near 66.5°, and were accompanied by reduced *E* region ionization (Figure 10d), which again suggests the formation of downward FAC there. In Figures 10e and 10f, an *E* region

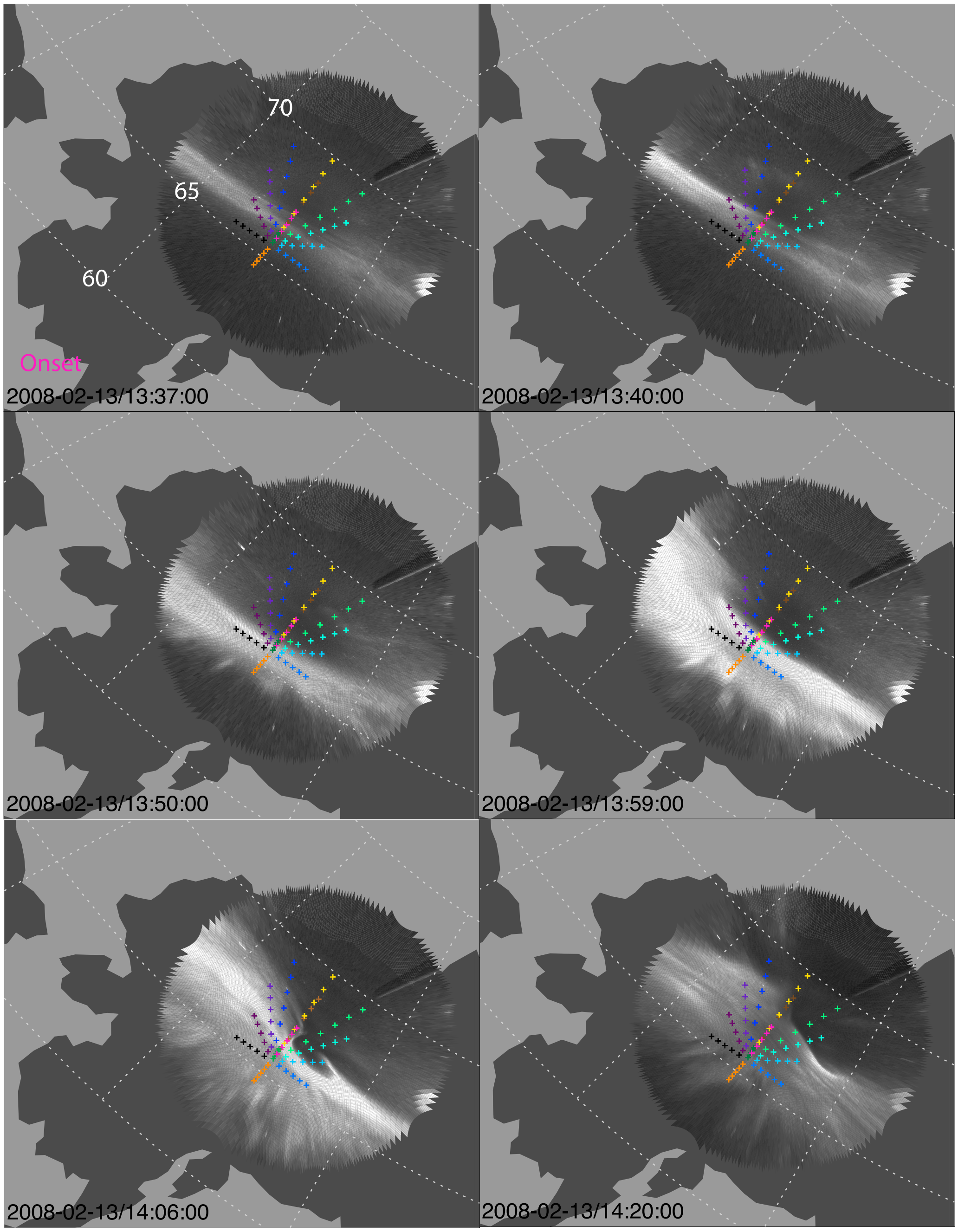

Figure 9. Selected auroral images observed by the ASI at Fort Yukon on 13 February 2008. The PFISR radar was located at ~2.55 MLT at 1337 UT in the postmidnight sector.

ionization increase, a signature of enhanced upward FAC, occurred just equatorward of these enhanced eastward flows. Therefore, these observations can be understood by the same argument as the previous event and again indicate that the downward FAC formed at onset was closed at least partially by the enhanced upward FAC in the Region 2 area.

[43] In Figure 9, the eastern edge of the aurora bulge intruded into the fov of the FYKN ASI at ~1359 UT. After that, intense ionizations appeared in beam 12 (Figure 10d) and at the same time that the eastward flows decreased to about 800 m/s (Figure 10b) and slightly rotated to a southeastward direction. In Figure 10g, the negative H bays at all stations indicate the prevailing westward electrojet overhead, and after the reappearance of the ionization, the H perturbation reached maximum. In this event, the Z component perturbation observed by the Poker Flat station changes sign after the intrusion, which could be attributed to the poleward shift of the center of westward electrojet. The transient signature in the D component is opposite to that in the previous event, which could be explained by the influence of localized downward FAC. Indeed, the image taken at 1406 UT exhibits an existence of a localized dark region embedded in bright auroras.

[44] *Senior et al.* [1982] presented six events of which magnetometer data were available from the TRIAD spacecraft and ionospheric conditions were monitored by the

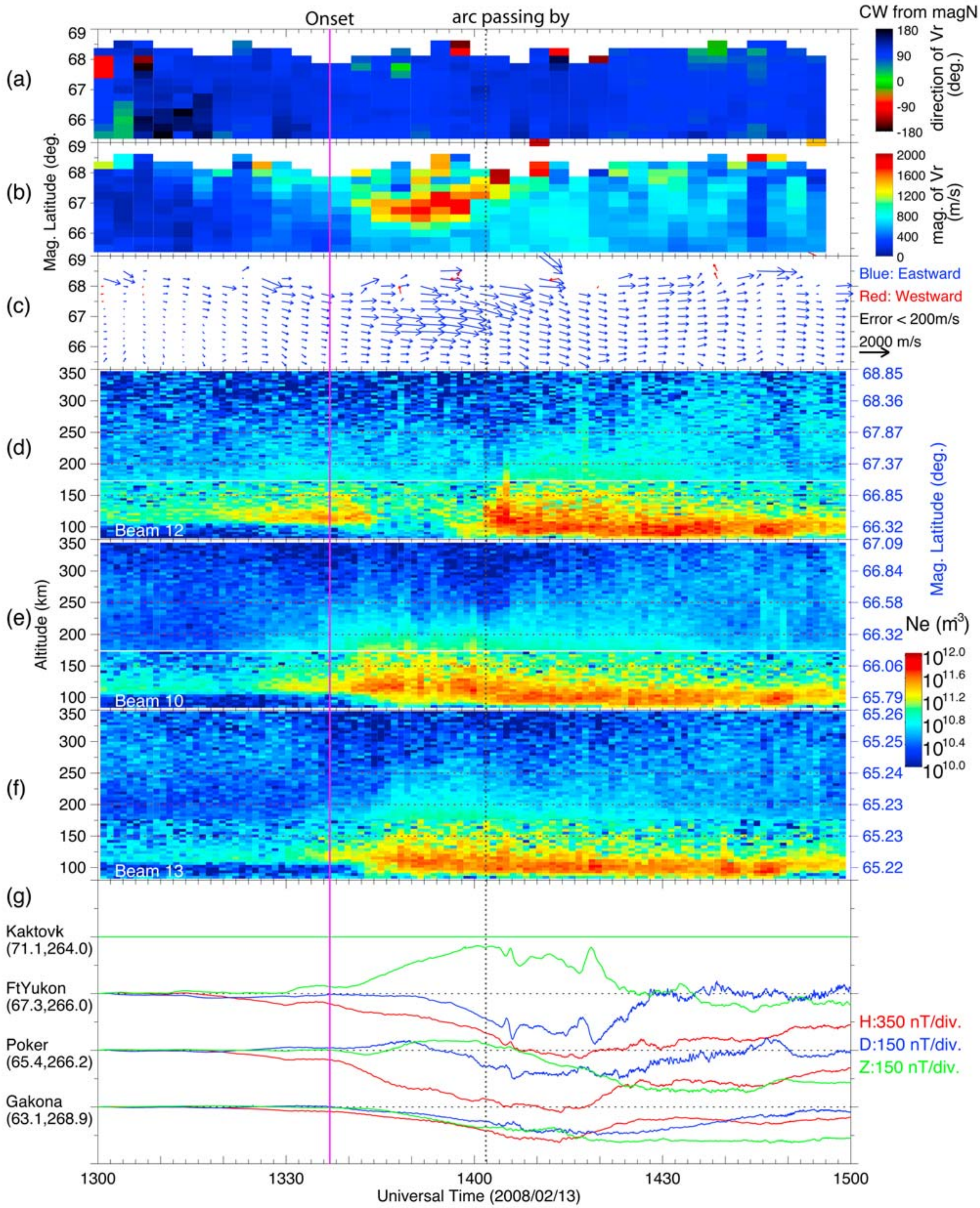

Figure 10. Same as Figure 3 but for the substorm at ∼1337 UT on 13 February 2008.

Chatanika radar. The authors found that the equatorward portion of the westward electrojet was dominated by a high conductivity and associated with upward Region 2 FAC, while its poleward portion was controlled by strong southward electric field and related with downward FAC. They further concluded that these FACs were connected by the southward Pedersen currents. *Kamide et al.* [1984] further analyzed two of the six events by adding observations from Alaska magnetometer and ASI. They pointed out that one was during the maximum epoch of a small substorm and the other was during the recovery phase. In addition, the authors noticed that the separation between the upward and downward FACs appear to coincide with the peak of the electric field. The observations presented in the above two papers are quite similar to what we presented in this section.

[45] However, the downward FACs observed in these studies were interpreted as the Region 1 FACs, while we suggest that those observed by PFISR belong to the substorm FAC system, which has the same polarity as the Region 1. Because the temporal resolution of the Chatanika radar measurement they used was ~13 min, it is difficult to determine dynamics of the downward FACs and to clearly identify what FAC system they belong to. By taking advantage of the high temporal resolution PFISR data, we are able to capture the formation of the downward FAC at the time of onset, which leads us to suggest that it is part of the newly formed substorm FAC system at onset instead of the permanent Region 1 FACs.

[46] During the ~90 radar runs, we have identified a total of 23 events in this category. As shown by the two examples in this section, a strong eastward flow channel was observed after the onset separating the enhanced upward FAC in the Region 2 area and the downward FAC of the SCW. For four events, when the prevailing convection was relatively high, counter clockwise flow shear was observed by the radar and the *E* region ionization decrease, as an indicator of downward FAC, extended to lower latitude and covered the whole radar *E* region fov. These counter clockwise flow shears are similar to those reported by *Kamide and Kokubun* [1996] and *Liang et al.* [2006]. For events during which the prevailing convection was relatively weak, only the equatorward portion of the enhanced flows developed in the radar fov and therefore only increased ionization was observed by the radar. When the eastern edge of the auroral bulge swept over the PFISR fov, the eastward flow enhancement was largely reduced and the *E* region ionization intensified in the previously depleted region. Concurrent observations from the Alaska magnetometer chain indicated intensification of the westward electrojet and the poleward shift of its center after the intrusion. These observations indicate a current closure relation between the downward substorm FAC and the upward Region 2 FAC, which are connected by the equatorward directed Pedersen currents.

3.3. Substorm Onset at the PFISR Local Time

[47] Due to the limited fov of the PFISR radar and the strong dependence of the ASI on local weather, there are very few substorm onsets that occurred right within the fovs of the radar and have optical data available at the same time. In this section, observations of two events are presented.

[48] On 27 March 2007, a full substorm following a pseudo breakup was captured by the ASI at FYKN (shown in Figure 11). In Figure 11, a thin east-west aligned growth phase arc was apparent in the image taken at 0920 UT. A pseudo breakup initiated near 0935 UT and was near the eastern portion of the ASI, as shown in the 0939 UT image. At ~0947 UT, the thin breakup arc of a full substorm onset occurred near 67° mlat, which further developed into very dynamic aurora forms. Observations from the POLAR UVI were also available during this period and further confirmed the timing and classifications of the pseudo breakup and the substorm.

[49] The concurrent PFISR and magnetometer observations are shown in Figure 12. The PFISR run for this day was in the 10-beam configuration. The convection flow data here were processed at ~2 min time resolution. The magenta line, once again, represents the substorm onset time. In Figures 12a and 12c, a very well defined Harang reversal signature can be seen. A star is denoted to represent the location of the breakup arc. It is clear that it occurred at the center of the Harang reversal. This observation is consistent with our previous observations presented by *Zou et al.* [2009]. After the onset, eastward flows poleward of the center of the shear show some brief enhancement, while the center of the shear continued moving equatorward until out of the radar fov. The equatorward moving westward flow region observed during the growth phase of this substorm and the flow relation to ionization signatures was discussed by *Lyons et al.* [2008], who found this flow region to be SAPS.

[50] The ionization enhancement in response to the substorm onset was apparent in all beams and persisted for a long time. In Figure 12d, during the early growth phase, there was enhanced ionization extending up to >250 km in beam 9, which indicates that beam 9 was continuously embedded within electron precipitation. However, homogeneous ionization confined to ~100–150 km (~65.3° mlat) altitude was recorded by beam 10. As discussed earlier, this seems to be a signature of proton precipitation. At ~0916 UT, the NOAA 17 satellite moved from lower latitudes to higher ones about 2.5 MLT west of the PFISR center meridian. Again, the energy flux carried by protons was observed to exceed that carried by electrons between ~65° to ~68.5° mlat and contributed to >95% of the total energy flux at the peak (not shown). This is consistent with our suggestion that the homogeneous ionization confined to ~100–150 km is due to proton precipitation.

[51] In Figure 12g, a large negative H bay was observed by the three stations at highest latitude after the onset, indicating influence of the westward electrojet. In contrast, the lowest station recorded positive perturbation. Thus, the magnetic Harang reversal, where the H perturbation equals zero, can be estimated to be slightly equatorward of Poker Flat (~65.4°), which is ~2° equatorward of the Harang reversal determined by the electric field, consistent with previous studies [*Kamide and Vickrey*, 1983; *Kunkel et al.*, 1986]. The sign reversal of the Z component observed by stations at Kaktovik and Fort Yukon after onset indicates the center of the westward electrojet was between them. On top of the general trend, there were lots of small scale variations in the magnetic perturbation, suggesting a highly dynamic ionospheric current system overhead.

[52] Another substorm onset captured by PFISR was on 4 September 2008. Observations from PFISR and magnetometers between 0620 and 0900 UT of this day are shown in Figure 13, in the same format as Figure 3. In Figure 13e, intense *E* region ionization initiated at ~0725 UT in beam 10, which was seen earlier than in the beams at the nearby latitudes and therefore marked the onset of the substorm. Electron density profiles from the northwest and northeast looking beams observed similar ionization profile, indicating the east-west extending of this onset arc. Although the

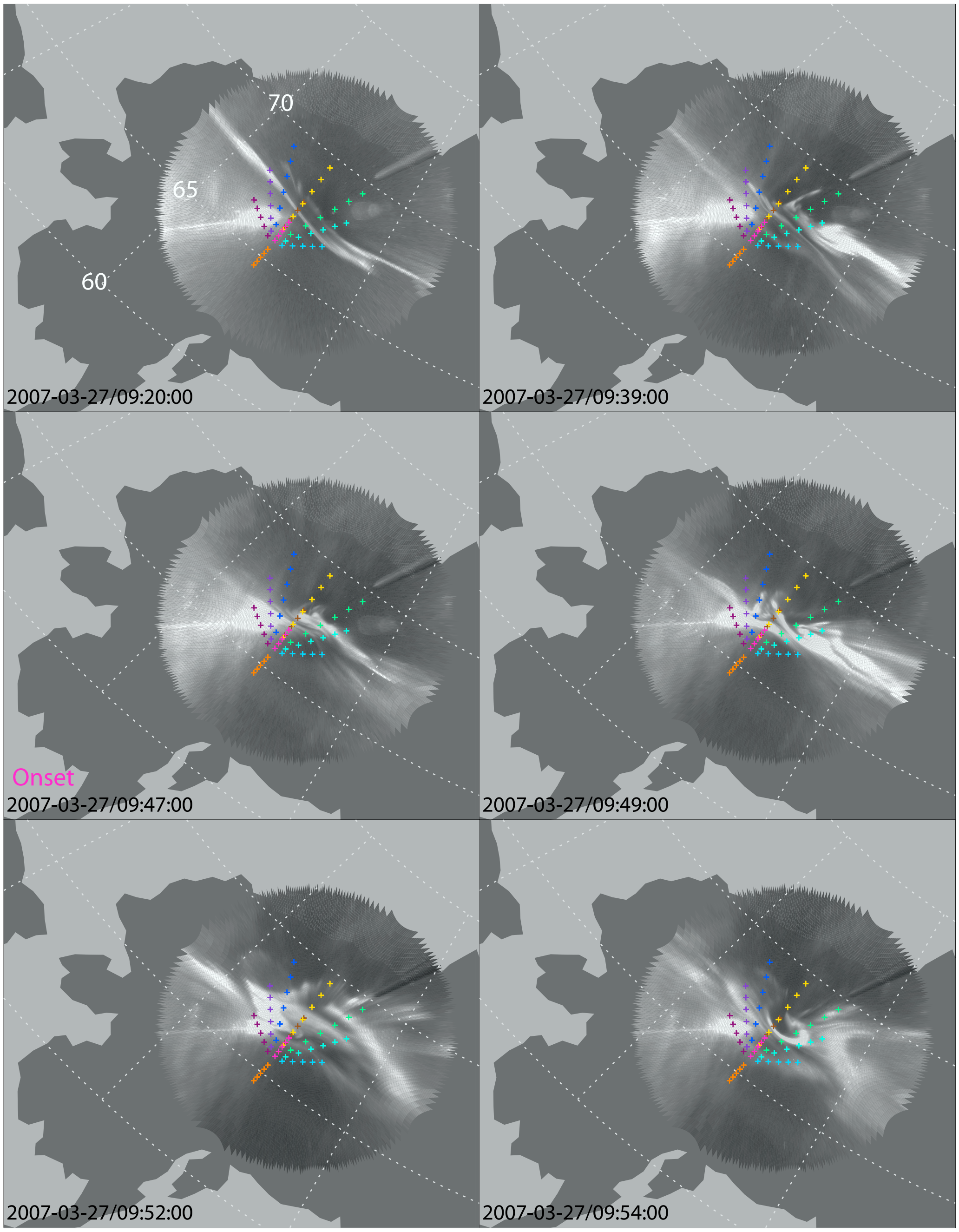

Figure 11. Selected auroral images observed by the ASI at Fort Yukon on 27 March 2007. The PFISR radar was located at ~22.7 MLT at 0947 UT in the premidnight sector.

sky was cloudy, the ASI at WHIT (12° east of PFISR center meridian) confirmed the onset timing determined based on the electron ionization profile and suggests that the onset arc extended westward from its fov.

[53] By comparing the ionization profile from the three central beams, it is clear that the onset initiated first in beam 10 near 66°. In Figure 13c, a star indicates the location of the onset arc. Similar to the previous event, the onset arc was located just in the center of the Harang reversal. The Harang reversal appeared in the radar fov about 10 min before the onset, probably resulting from equatorward movement from latitudes beyond the radar fov. After the onset, the weak westward flows below 66° mlat changed to southeastward, indicating a relaxation of the flow shear at this latitude and the shear probably moved further equatorward, as has been seen by previous observations [*Bristow and Jensen*, 2007; *Zou et al.*, 2009]. The southeastward flows continued until ~0818 UT, when they changed to southwestward and their magnitude reduced. Meanwhile, the ionization profile in all three beams suddenly and significantly reduced. This transition probably marked the end of the recovery phase of this substorm and the convection flows returned to the prevailing direction, which is normally westward at this local time.

[54] In Figure 13g, there were significant magnetic perturbations associated with onset. Within the first few

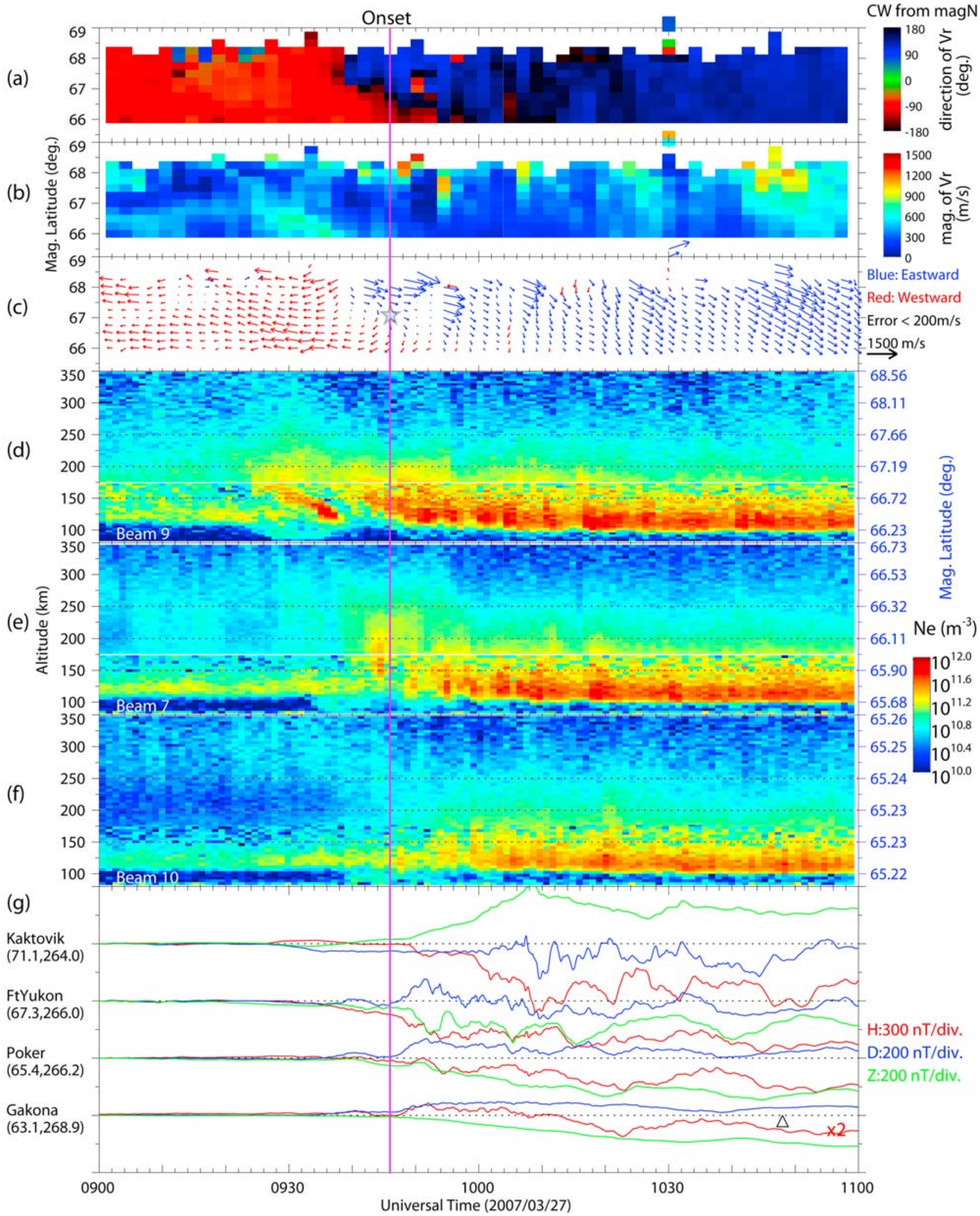

Figure 12. Same as Figure 3 but for the substorm at ∼0946 UT on 27 March 2007.

min around onset, the perturbation in the Z component observed at Fort Yukon was positive, while that observed at Poker Flat was negative. This indicates the center of the westward electrojet was between these two stations. Around 0730 UT, the Z component perturbation at Fort Yukon changed to negative. This, together with the positive Z component perturbation at Kaktovik, suggests the center of the westward electrojet shifted poleward and was between the two highest latitude stations. Three high latitude stations show negative H perturbation throughout the whole period.

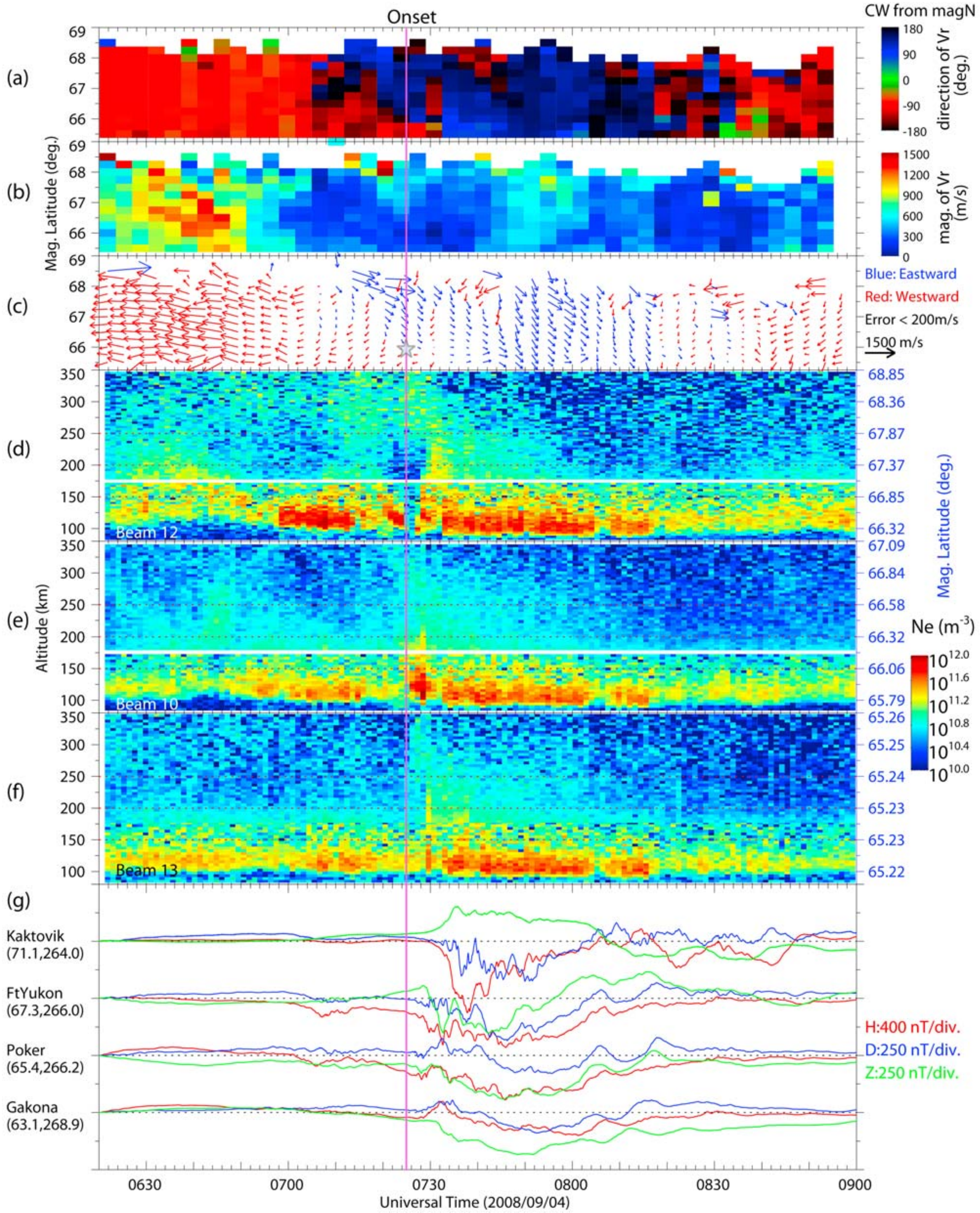

Figure 13. Same as Figure 3 but for the substorm at ∼0725 UT on 4 September 2008.

In contrast, Gakona, the station at lowest altitude, first recorded positive H perturbation and then negative perturbation, which implies that the magnetic Harang reversal was initially between Poker Flat and Gakona, and then shifted equatorward. Together with the flow observation, this suggests that the magnetic Harang reversal was again a couple of degrees equatorward of that determined by electric fields.

[55] The small fov of the radar limits the number of events available for this category. Nevertheless, we found a

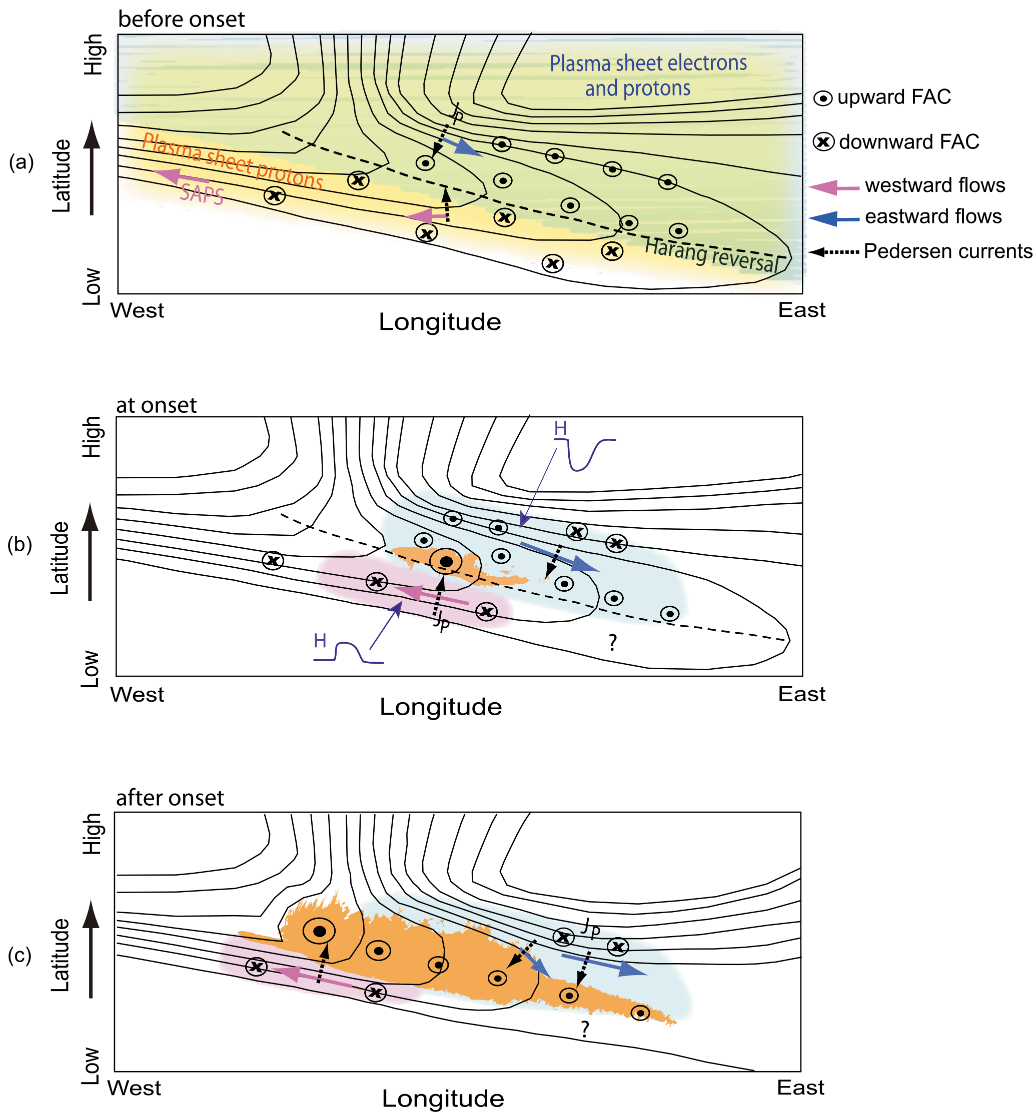

Figure 14. Schematic diagrams of equipotentials, convection flows, and currents near the Harang reversal region (a) before, (b) at, and (c) after substorm onset.

total of 11 events for which the onset arc was located either within (6) or poleward (5) of the PFISR fov. For the first situation, the onset was observed to be within the Harang reversal for five events, including a pseudo breakup, while the other onset was found to occur in a counter clockwise flow shear in the postmidnight sector, which formed at the onset of a previous substorm.

[56] For events that occurred poleward of PFISR, the Harang reversal was observed a few minutes after onset for four events, which is probably due to equatorward motion of the Harang reversal after onset, as have been shown by *Bristow and Jensen* [2007] and in Figure 8 of *Zou et al.* [2009]. A rather weak shear with equatorward flows instead of eastward flows was seen for the other event.

4. Two-Dimensional Features of Substorm Ionospheric Electrodynamics

[57] The results presented in the previous section, together with those of *Zou et al.* [2009], lead us to produce the schematic plot of electrodynamical features and their evolution associated with the expansion phase of substorms shown in Figure 14. From top to bottom, each diagram represents ionospheric equipotentials, flows and FACs before, at, and after onset in geomagnetic coordinates. The x axis represents the east-west span of the Harang reversal extending approximately a few hours of MLT and the y axis covers roughly several degrees in latitude. Note that this is just a schematic plot and the latitudinal and MLT coverage for individual events should be highly variable. In each diagram, solid arrows, either magenta or blue, denote the convection flows, dashed black arrows denote the Pedersen currents, and circles with dot (cross) represent upward (downward) FAC.

[58] In Figure 14a, a well-defined Harang reversal can be seen, which is slightly tilted toward lower latitudes at later local times, and the dashed line highlights the center of the shear. The equipotentials shown in Figure 14a are adopted from an RCM simulation [*Gkioulidou et al.*, 2009]. Yellow shading roughly represents the region of proton precipita-

tion, while blue shading roughly represents that of electron precipitation. As shown, the electron and proton precipitation regions overlap each other except for a narrow wedge-shaped region at lower latitude. Within this low-latitude region, proton precipitation extends equatorward of the equatorward boundary of electron precipitation and SAPS are often observed. Based on the RCM simulations, upward Region 2 FACs are approximately distributed poleward of the Harang shear while downward Region 2 FACs are roughly equatorward of it. In other words, the Region 2 FACs change direction near, although not exactly at the center of, the reversal [*Gkioulidou et al.*, 2009]. Consistent with the RCM results, the downward Region 2 currents equatorward of the reversal have been observed by low-altitude polar-orbiting satellites [*Anderson et al.*, 2001].

[59] In Figure 14b, the breakup arc of onset, represented by the orange shaded region, is placed at the center of the Harang reversal, based on observations from section 3.3 and those of *Zou et al.* [2009]. Enhanced westward flows, represented by a larger magenta arrow, are observed equatorward of the onset region [*Zou et al.*, 2009], including the WTS, which has not yet had time to move westward. Based on the observations described in section 3.2, an enhanced eastward flow channel, denoted by the larger blue arrow, forms east of the breakup arc at onset. *E* region ionization decreases poleward of this flow channel and increases equatorward of it, indicating, respectively, formation of downward FAC of the SCW and strengthening of the upward FAC in the Region 2 area. The flow-ionization relation suggests that the downward FAC formed at onset is at least partially closed by the upward region 2 FAC via equatorward directed Pedersen currents. Occasionally, a counter clockwise vortex can be seen in this region. As discussed in section 3.3, observations from the magnetometers distributed around PFISR show that a positive H perturbation is frequently observed by stations southward and/or westward of the onset (pink shaded region), while a more prominent negative H perturbation is observed by stations located near, poleward and/or eastward of the onset (light blue shaded region). These H perturbations reflect, respectively, the enhanced eastward and westward auroral electrojets in these two regions at onset. The magnetic Harang reversal, e.g., the boundary separating the pink and blue shaded regions, is found to be a couple of degrees equatorward of that determined by the electric fields, which is probably an indication of the imbalance between the westward and the eastward electrojet strengths. Of course, the FAC in this region might also contribute to this discrepancy. The region further equatorward of the upward Region 2 and east of onset is usually not covered by the PFISR fov and therefore the ionospheric responses to the substorm onset is not covered in the present study.

[60] Frequently, the onset arc is observed to break up from or very near an existing growth phase arc, which implies that the growth phase arc should also be very close to the center of the Harang reversal at this MLT. However, since growth phase arcs can extend a few hours of MLT in the horizontal direction, the question arises of what is the relative location of growth phase arcs to that of the Harang shear versus MLT. In the current study, 1-D measurement of a single case cannot address this question and the IMAGE observations used by *Zou et al.* [2009] did not have high enough spatial resolution for revealing the fine structure of the growth phase arcs. Therefore, this is still an open question.

[61] As shown in Figure 14c, after substorm onset, brightened aurora expands latitudinally as well as azimuthally and forms an auroral bulge. As shown in sections 3.2 and 3.3, shear flows become more meridionally aligned in regions where the aurora expansion reaches and ionization is enhanced. Usually, the WTS moves westward, and in section 3.1 we have shown that westward flows equatorward of the WTS increase. These westward flows are in the subauroral region and could extend throughout the region of almost pure proton precipitation to the transition region where electron precipitation gradually increases. In section 3.1, the observation that significantly intensified *E* region ionization is observed poleward of the enhanced westward flows suggests at least part of the upward FAC associated with the WTS is closed by the poleward Pedersen currents fed by the lower-latitude downward Region 2 FAC. There is also evidence from the SuperDARN radars for the formation of a clockwise vortex associated with the leading edge of the WTS [*Zou et al.*, 2009]. Whether this is a persistent feature needs further investigation. In the region of substorm downward FACs, as shown in section 3.3, the ionization decrease is terminated by the intrusion of the eastward moving auroral bulge. Meanwhile, previously enhanced eastward flows suddenly decrease and are often accompanied by a rotation to a southeastward direction, indicating an increase of westward electric field.

[62] Note that this is a general schematic sketch of substorm signatures based on limited number of isolated substorm events and is not meant to encompass all features for all cases. In addition, electric equipotentials shown in Figures 14b and 14c have been modified from those in Figure 14a based on observations and are not from the RCM simulation. In this paper, we qualitatively discussed the current closure relation between the Region 2 FAC and the FAC of the SCW that forms at onset. Quantitative study of to what extent the Region 2 FAC contribute to the closure of the substorm FAC would be interesting, but requires utilization of comprehensive model calculations and is beyond the scope of this paper. In addition, due to the relatively limited radar fov, the more poleward permanent Region 1 current system has not been discussed here and thus not included in Figure 14.

5. Summary and Conclusions

[63] In this paper, we utilized the newly available PFISR radar, the surrounding ground-based ASIs and magnetometers, and spacecraft to study the nightside ionospheric electrodynamics associated with substorms. Convection flow evolution, ionization and ground magnetic perturbation west of, at, and east of the onset were discussed separately and extensively. By synthesizing the observations from each category and features described previously by *Zou et al.* [2009], a 2-D picture of the evolution of ionospheric electrodynamics covering a broad region of MLT was constructed for the substorm expansion phase. The current results not only show consistency with previous observations but also reveal many new aspects. The observations are summarized as follows:

[64] 1. Weak and homogeneous ionization confined to the *E* region (100–150 km) are frequently observed during the growth phase. This is evidence for precipitating energetic protons, which is supported by low-altitude polar-orbiting satellite observations. The region where almost pure proton precipitation is observed is usually in the evening sector and equatorward of the equatorial boundary of electron precipitations.

[65] 2. West of onset, westward flows near the equatorward portion of the PFISR fov increase in response to the passage of the WTS poleward of them. A delay of the westward flow enhancement was seen for the one event having onset well to the east of PFISR. Meanwhile, significant *E* region ionization increases occur poleward of the westward flow enhancement and within the WTS, which indicates that the poleward Pedersen currents contribute at least partially to the current closure of the upward FAC associated with the WTS. These poleward Pedersen currents should be closed by the downward Region 2 FAC further equatorward of them. The enhanced westward flows extend throughout the almost purely proton precipitation region of SAPS to the transition region between the electron and pure proton precipitation regions.

[66] 3. Eastward of onset, an enhanced eastward flow channel is observed and accompanied by *E* region ionization depletion poleward of the peak flows, indicating the formation of downward FAC of the SCW at onset. On the other hand, ionization further increases equatorward of the peak flow and equatorward of the downward FAC, indicating strengthening of the Region 2 upward FAC. This, together with the observed flow enhancement, suggests that the downward FAC formed at onset feeds the more equatorward upward FAC in the Region 2 region via equatorward Pedersen currents.

[67] Enhanced eastward flows start to decrease when the eastern edge of the auroral bulge intrudes into the radar fov from the west, the intrusion being associated with ionization enhancement. Although the electric fields decrease, the enhancement of the *E* region ionization leads to an increase of the westward electrojet, as indicated by the observation that the negative H bay reaches maximum after the intrusion.

[68] 4. For events occurring within the radar meridian, 10 out of 11 events were found to be associated with the Harang reversal. In particular, five out of the six events for which the onset occurred within the radar fov show that the breakup arc was located within the center of the Harang reversal. Frequently, the magnetic Harang reversal occurs a couple of degrees equatorward than that determined from the electric field, consistent with previous studies. Occasionally, almost pure proton precipitation was observed slightly equatorward of the breakup arc before onset.

[69] Overall, by combining observations of these three categories together, we have qualitatively determined a relation between the substorm FAC system and the Region 2 FAC system. The radar observations provide a unique perspective of substorm electrodynamics, and give fundamental information that we believe is necessary for full understanding of the substorm process.

[70] **Acknowledgments.** This work at UCLA was supported by NSF grants ATM-0639312 and ATM-0646233. The PFISR measurements and analysis are supported under cooperative agreements ATM-0608577 between the U.S. NSF and SRI International. We thank the Geophysical Institute of the University of Alaska Fairbanks for providing the Alaska magnetometer data, the NOAA's National Geophysical Data Center for providing the NOAA satellite data, and the principal investigator for the Polar UVI experiment, G. K. Parks.

[71] Amitava Bhattacharjee thanks Tsugunobu Nagai and Jesper Gjerloev for their assistance in evaluating this paper.

References

Akasofu, S.-I., D. S. Kimball, and C.-I. Meng (1965), Dynamics of the aurora, II, Westward traveling surges, *J. Atmos. Terr. Phys.*, *27*, 173, doi:10.1016/0021-9169(65)90114-5.

Akasofu, S.-I., C.-I. Meng, and D. S. Kimball (1966), Dynamics of the aurora, IV, Polar magnetic substorm and westward traveling surges, *J. Atmos. Terr. Phys.*, *28*, 489, doi:10.1016/0021-9169(66)90058-4.

Anderson, P. C., W. B. Hanson, R. A. Heelis, J. D. Craven, D. N. Baker, and L. A. Frank (1993), A proposed production model of rapid subauroral ion drifts and their relationship to substorm evolution, *J. Geophys. Res.*, *98*(A4), 6069–6078, doi:10.1029/92JA01975.

Anderson, P. C., I. W. McCrea, D. J. Strickland, J. B. Blake, and M. D. Looper (1997), Coordinated EISCAT/DMSP measurements of electron density and energetic electron precipitation, *J. Geophys. Res.*, *102*(A4), 7421–7430, doi:10.1029/96JA03824.

Anderson, P. C., et al. (2001), Multisatellite observations of rapid subauroral ion drifts (SAID), *J. Geophys. Res.*, *106*, 29,585–29,599.

Baumjohann, W., R. J. Pellinen, H. J. Opgenoorth, and E. Nielsen (1981), Joint two-dimensional observations of ground magnetic and ionospheric electric fields associated with auroral zone currents: Current systems associated with local auroral breakup, *Planet. Space Sci.*, *29*, 431, doi:10.1016/0032-0633(81)90087-8.

Borovsky, J. E. (1993), Auroral arc thicknesses as predicted by various theories, *J. Geophys. Res.*, *98*(A4), 6101–6138, doi:10.1029/92JA02242.

Bristow, W. A., and P. Jensen (2007), A superposed epoch study of SuperDARN convection observations during substorms, *J. Geophys. Res.*, *112*, A06232, doi:10.1029/2006JA012049.

Bristow, W. A., A. Otto, and D. Lummerzheim (2001), Substorm convection patterns observed by the Super Dual Auroral Radar Network, *J. Geophys. Res.*, *106*, 24,593–24,609, doi:10.1029/2001JA000117.

Bristow, W. A., G. Sofko, H. C. Stenbaek-Nielsen, S. Wei, D. Lummerzheim, and A. Otto (2003), Detailed analysis of substorm observations using SuperDARN, UVI, ground-based magnetometers, and all-sky imagers, *J. Geophys. Res.*, *108*(A3), 1124, doi:10.1029/2002JA009242.

Clauer, C. R., and R. L. McPherron (1974), Mapping the local time-universal time development of magnetospheric substorms using mid-latitude magnetic observations, *J. Geophys. Res.*, *79*(19), 2811–2820, doi:10.1029/JA079i019p02811.

Donovan, E., et al. (2006), The THEMIS all-sky imaging array-system design and initial results from the prototype imager, *J. Atmos. Sol. Terr. Phys.*, *68*, 1472, doi:10.1016/j.jastp.2005.03.027.

Erickson, G. M., R. W. Spiro, and R. A. Wolf (1991), The physics of the Harang discontinuity, *J. Geophys. Res.*, *96*, 1633–1645, doi:10.1029/90JA02344.

Foster, J. C., and W. J. Burke (2002), SAPS: A new characterization for sub-auroral electric fields, *Eos Trans. AGU*, *83*, 393–394, doi:10.1029/2002EO000289.

Fujii, R., R. A. Hoffman, P. C. Anderson, J. D. Craven, M. Sugiura, L. A. Frank, and N. C. Maynard (1994), Electrodynamic parameters in the nighttime sector during auroral substorms, *J. Geophys. Res.*, *99*(A4), 6093–6112, doi:10.1029/93JA02210.

Galand, M., and A. D. Richmond (2001), Ionospheric electrical conductances produced by auroral proton precipitation, *J. Geophys. Res.*, *106*(A1), 117–125, doi:10.1029/1999JA002001.

Gjerloev, J. W., and R. A. Hoffman (2002), Currents in auroral substorms, *J. Geophys. Res.*, *107*(A8), 1163, doi:10.1029/2001JA000194.

Gjerloev, J. W., R. A. Hoffman, E. Tanskanen, M. Friel, L. A. Frank, and J. B. Sigwarth (2003), Auroral electrojet configuration during substorm growth phase, *Geophys. Res. Lett.*, *30*(18), 1927, doi:10.1029/2003GL017851.

Gkioulidou, M., C.-P. Wang, L. R. Lyons, and R. A. Wolf (2009), Formation of the Harang reversal and its dependence on plasma sheet conditions: RCM simulations, *J. Geophys. Res.*, *114*, A07204, doi:10.1029/2008JA013955.

Harang, L. (1946), The mean field of disturbance of polar geomagnetic storms, *Terr. Magn. Atmos. Electr.*, *51*(3), 353–380, doi:10.1029/TE051i003p00353.

Heinselman, C. J., and M. J. Nicolls (2008), A Bayesian approach to electric field and E region neutral wind estimation with the Poker Flat Advanced Modular Incoherent Scatter Radar, *Radio Sci.*, *43*, RS5013, doi:10.1029/2007RS003805.

Heppner, J. P. (1972), The Harang discontinuity in auroral belt ionospheric currents, *Geophys. Publ.*, *29*, 105–120.
Hoffman, R. A., R. Fujii, and M. Sugiura (1994), Characteristics of the field-aligned current system in the nighttime sector during auroral substorms, *J. Geophys. Res.*, *99*(A11), 21,303–21,325, doi:10.1029/94JA01659.
Iijima, T., and T. A. Potemra (1978), Large-scale characteristics of field-aligned currents associated with substorms, *J. Geophys. Res.*, *83*(A2), 599–615, doi:10.1029/JA083iA02p00599.
Inhester, B., W. Baumjohann, R. A. Greenwald, and E. Nielsen (1981), Joint two-dimensional observations of ground magnetic and ionospheric electric fields associated with auroral zone currents, *J. Geophys.*, *49*, 155–162.
Kamide, Y., and S. Kokubun (1996), Two-component auroral electrojet: Importance for substorm studies, *J. Geophys. Res.*, *101*, 13,027–13,046, doi:10.1029/96JA00142.
Kamide, Y., and J. F. Vickrey (1983), Variability of the Harang discontinuity as observed by the Chatanika radar and the IMS Alaska magnetometer chain, *Geophys. Res. Lett.*, *10*(2), 159–162, doi:10.1029/GL010i002p00159.
Kamide, Y., R. M. Robinson, S.-I. Akasofu, and T. A. Potemra (1984), Aurora and electrojet configuration in the early morning sector, *J. Geophys. Res.*, *89*(A1), 389–393, doi:10.1029/JA089iA01p00389.
Kirkwood, S., H. J. Opgenoorth, and J. S. Murphree (1988), Ionospheric conductivities, electric fields, and currents associated with auroral substorms measured by the EISCAT radar, *Planet. Space Sci.*, *36*, 1359, doi:10.1016/0032-0633(88)90005-0.
Kunkel, T., W. Baumjohann, J. Untiedt, and R. Greenwald (1986), Electric fields and currents at the Harang discontinuity: A case study, *J. Geophys.*, *59*, 73–86.
Liang, J., G. J. Sofko, and H. U. Frey (2006), Postmidnight convection dynamics during substorm expansion phase, *J. Geophys. Res.*, *111*, A04205, doi:10.1029/2005JA011483.
Lilensten, J., and M. Galand (1998), Proton-electron precipitation effects on the electron production and density above EISCAT (Tromsø) and ESR, *Ann. Geophys.*, *16*, 1299–1307, doi:10.1007/s00585-998-1299-8.
Lyons, L. R., S. Zou, C. J. Heinselman, M. J. Nicolls, and P. Anderson (2008), Poker flat radar observations of the magnetosphere-ionosphere coupling electrodynamics of the earthward penetrating plasma sheet following convection enhancements, *J. Atmos. Sol. Terr. Phys.*, doi:10.1016/j.jastp.2008.09.025.
Marklund, G. T., et al. (1998), Observations of the electric field fine structure associated with the westward traveling surge and large-scale auroral spirals, *J. Geophys. Res.*, *103*(A3), 4125–4144, doi:10.1029/97JA00558.
McPherron, R. L. (1970), Growth phase of magnetospheric substorms, *J. Geophys. Res.*, *75*(28), 5592–5599, doi:10.1029/JA075i028p05592.
Mende, S. B., S. E. Harris, H. U. Frey, V. Angelopoulos, C. T. Russell, E. Donovan, B. Jackel, M. Greffen, and L. M. Peticolas (2008), The THEMIS array of ground-based observatories for the study of auroral substorms, *Space Sci. Rev.*, doi:10.1007/s11214-008-9380.
Miyashita, Y., et al. (2008), Response of large-scale ionospheric convection to substorm expansion onsets: A case study, *J. Geophys. Res.*, *113*, A12309, doi:10.1029/2008JA013586.
Nielsen, E., and R. A. Greenwald (1979), Electron flow and visual aurora at the Harang discontinuity, *J. Geophys. Res.*, *84*(A8), 4189–4199, doi:10.1029/JA084iA08p04189.
Opgenoorth, H. J., R. J. Pellinen, W. Baumjohann, E. Nielsen, G. Marklund, and L. Eliasson (1983), Three-dimensional current flow and particle precipitation in a westward traveling surge (observed during the Barium-Geos rocket experiment), *J. Geophys. Res.*, *88*, 3138–3152, doi:10.1029/JA088iA04p03138.
Paschmann, G., S. Haaland, and R. Treumann (Eds.) (2002), *Auroral Plasma Physics*, *Space Sci. Rev.*, vol. 103(nos. 1–4), Springer, New York.
Rees, M. H. (1963), Auroral ionization and excitation by incident energetic electrons, *Planet. Space Sci.*, *11*, 1209–1218, doi:10.1016/0032-0633(63)90252-6.
Robinson, R. M., and R. R. Vondrak (1985), Characteristics and sources of ionization in the continuous aurora, *Radio Sci.*, *20*(3), 447–455, doi:10.1029/RS020i003p00447.
Robinson, R. M., and R. R. Vondrak (1990), Electrodynamic properties of auroral surges, *J. Geophys. Res.*, *95*(A6), 7819–7832, doi:10.1029/JA095iA06p07819.
Robinson, R. M., F. Rich, and R. R. Vondrak (1985), Chatanika radar and S3–2 measurements of auroral zone electrodynamics in the midnight sector, *J. Geophys. Res.*, *90*(A9), 8487–8499, doi:10.1029/JA090iA09p08487.
Rostoker, G. (1972), Polar magnetic substorms, *Rev. Geophys.*, *10*(1), 157–211, doi:10.1029/RG010i001p00157.
Rostoker, G., and J. L. Kisabeth (1973), Response of the polar electrojets in the evening sector to polar magnetic substorms, *J. Geophys. Res.*, *78*(25), 5559–5571, doi:10.1029/JA078i025p05559.
Senior, C., R. M. Robinson, and T. A. Potemra (1982), Relationship between field-aligned currents, diffuse auroral precipitation and the westward electrojet in the early morning sector, *J. Geophys. Res.*, *87*(A12), 10,469–10,477, doi:10.1029/JA087iA12p10469.
Senior, C., J. R. Sharber, O. de la Beaujardière, R. A. Heelis, D. S. Evans, J. D. Winningham, M. Sugiura, and W. R. Hoegy (1987), *E* and *F* region study of the evening sector auroral oval: A Chatanika/Dynamics Explorer 2/NOAA 6 comparison, *J. Geophys. Res.*, *92*(A3), 2477–2494, doi:10.1029/JA092iA03p02477.
Sergeev, V. A., L. I. Vagina, R. D. Elphinstone, J. S. Murphree, D. J. Hearn, L. L. Cogger, and M. L. Johnson (1996), Comparison of UV optical signatures with the substorm current wedge as predicted by an inversion algorithm, *J. Geophys. Res.*, *101*(A2), 2615–2627, doi:10.1029/95JA00537.
Smirnova, N. V., A. N. Lyakhov, Y. I. Setzer, A. P. Osepian, C. I. Meng, R. Smith, and H. C. Stenbaek-Nielsen (2004), Precipitating protons and their role in ionization of the polar ionosphere, *Cosmic Res., Engl. Transl.*, *42*, 210–218, doi:10.1023/B:COSM.0000033296.08433.94.
Tighe, W. G., and G. Rostoker (1981), Characteristics of westward traveling surges during magnetic substorms, *J. Geophys.*, *50*, 51–67.
Weygand, J. M., R. L. McPherron, H. Frey, O. Amm, K. Kauristie, A. T. Viljanen, and A. Koistinen (2008), Relation of substorm onset to Harang discontinuity, *J. Geophys. Res.*, *113*, A04213, doi:10.1029/2007JA012537.
Zou, S., L. R. Lyons, C.-P. Wang, A. Boudouridis, J. M. Ruohoniemi, P. C. Anderson, P. L. Dyson, and J. C. Devlin (2009), On the coupling between the Harang reversal evolution and substorm dynamics: A synthesis of SuperDARN, DMSP, and IMAGE observations, *J. Geophys. Res.*, *114*, A01205, doi:10.1029/2008JA013449.

C. J. Heinselman and M. J. Nicolls, Center for Geospace Studies, SRI International, Menlo Park, CA 94025, USA.

L. R. Lyons and S. Zou, Department of Atmospheric and Oceanic Sciences, University of California, Los Angeles, CA 90095, USA. (sha@atmos.ucla.edu)

S. B. Mende, Space Sciences Laboratory, University of California, Berkeley, CA 94720, USA.